EG&G Idaho, Inc.

FORM EG&G-398
(Rev. 05-79)

INTERIM REPORT

Accession No. _____

Report No. EGG-TFBP-5250

Contract Program or Project Title: Thermal Fuels Behavior Program

Subject of this Document: FRAP-T5: A Review of Thermal and Mechanical Analysis and Performance

Type of Document: Topical Report

Author(s): S. L. Seiffert, A. D. Appelhans

Date of Document: September 1980

Responsible NRC Individual and NRC Office or Division: G. P. Marino, Reactor Safety Research

EG&G Idaho, Inc.
Idaho Falls, Idaho 83401

Prepared for the
U.S. Nuclear Regulatory Commission
Washington, D.C.
Under DOE Contract No. DE-AC07-76IDC1570
NRC FIN No. A6041

INTERIM REPORT

FRAP-T5: A REVIEW OF THERMAL AND MECHANICAL ANALYSIS AND PERFORMANCE

by

S. L. Seiffert A. D. Appelhans

September 1980

Approved:

R R Hobbins

R. R. Hobbins, Manager
Program Development and Evaluation Branch

P. E. MacDonald

P. E. MacDonald, Manager
Light Water Reactor Fuel Research Division

Reviewed By:

E T Laats

E. T. Laats, Supervisor
Fuel Assessment and Analysis Section

T. M. Howe

T. M. Howe, Manager
Fuel Analysis Research and Development Branch

FOREWORD

The main purpose of the Thermal Fuels Behavior Program is to understand the behavior of light water reactor fuel during postulated accidents and operational transients. The FRAP-T code is designed to calculate thermal, mechanical, and chemical interaction response of the fuel rod during such events. This report presents an assessment of FRAP-T5, by comparing data from recent tests with posttest code calculations, and by qualitatively evaluating the code from an "experimenter's" point of view.

The planning of each test depends on the FRAP-T pretest calculations. Improvement of individual models in the code necessarily has its basis in the measured data and the observed physical phenomena resulting from the tests. However, elapsed time from the test planning stage until qualified test data and postirradiation examination results are available may be significant. As a consequence, an assessment of the "code simulation capability" by comparison of pretest calculations with data loses significance. Such an evaluation becomes particularly difficult when the intended test conditions are somewhat different than the test rod environment actually accomplished during the test. Therefore, a posttest comparison calculation is essential in order to make an assessment of the capability of the code to simulate fuel behavior.

Discrepancies between the fuel behavior parameters calculated by the FRAP-T5 code and selected experimental data are reviewed. The comparisons available for review are limited. Descriptions of physical phenomena from tests important to determining fuel behavior under transient conditions have also been assembled. As more test results are qualified and newer versions of FRAP-T are published, evaluation of the transient calculational capability of the code on the basis of test observations, will continue.

ACKNOWLEDGEMENTS

The authors thank Dr. R. R. Hobbins, Dr. D. W. Croucher and P. E. MacDonald for their technical review of this report. Special thanks is extended to E. T. Laats of the Fuel Assessment and Analysis Section, and L. J. Siefken and T. M. Howe of the Fuel Analysis Research and Development Branch for their technical review and comments.

ABSTRACT

A review of the ability of the Fuel Rod Analysis Program-Transient (FRAP-T) computer code to predict fuel rod behavior is presented. Fuel rod behavior calculations were compared with data from long term irradiation tests on instrumented fuel assemblies conducted in the Halden, Norway, Heavy Boiling Water Reactor to study the effects of fuel rod internal pressure and gas composition on thermal gap conductance. Fuel rod thermal and mechanical behavior calculations were compared with data from a hypothetical reactivity initiated accident transient test performed in the Power Burst Facility reactor to determine fuel rod failure data.

SUMMARY

The ability of the Fuel Rod Analysis Program-Transient (FRAP-T) computer code to calculate the thermal and mechanical behavior of test fuel rods is discussed. The purpose of this report is to examine the performance of FRAP-T5. Emphasis is placed on a qualitative review of the code performance by comparison of in-pile data and postirradiation examination measurements with computer code calculations.

Fuel behavior studies performed in the Halden, Norway, Heavy Boiling Water Reactor, provided information about the effect of fill gas pressure and composition of fuel thermal performance under steady state conditions. A review of the fuel rod thermal models used in FRAP-T5 showed that the code in general predicts the thermal response of the fuel to changes in gas composition ranging from 0 to 10% Xe in He and in rod internal pressure from 0.1 to 5.0 MPa. One exception was noted for a rod with large fuel-cladding gas gap, where above about 2.0 MPa and >10% Xe concentration, the measured fuel thermal behavior exhibited an unexpected trend.

An analysis and interpretation of results from the reactivity initiated accident test (RIA), Test RIA 1-1, conducted in the Power Burst Facility Reator to determine the extent of fuel rod damage and modes of fuel rod failure are presented. The test fuel rod behavior was assessed using comparisons of FRAP-T5 calculated behavior with instrumentation response data and from posttest metallurgical observations.

The FRAP-T5 calculated rod temperature histories emphasized that the mode of fuel rod failure for rods tested at 285 cal/g during an RIA event at BWR hot start-up conditions was strongly affected by the peak fuel enthalpy. Peak fuel centerline temperatures calculated by FRAP-T5 were in general agreement with the measured values, although the amount of fuel melting was overpredicted. Calculated cladding surface temperatures were overpredicted, indicating that effects, such as the cooling fin effect, not currently modeled in FRAP-T5, were significant.

Pellet-cladding mechanical interaction induced failure due to high strain rate deformation was correctly indicated by the FRAP-T5 calculated thermal-mechanical history. Some variations in the calculated deformation and elongation behavior suggest that the code has some modeling deficiences in describing the very rapid changes in fuel rod behavior induced by an RIA.

CONTENTS

FIGURES

TABLES

1. INTRODUCTION

The safe operation of light water reactors (LWRs) requires an ability to accurately predict the performance of nuclear fuels in order to assure the integrity of reactor core components under normal operation and hypothesized accident conditions. To achieve this capability, the U.S. Nuclear Regulatory Commission (NRC) has sponsored an extensive program of analytical code development and assessment. The computer code being developed for the prediction of transient fuel rod response under hypothetical accident conditions is the Fuel Rod Analysis Program-Transient (FRAP-T) code.[1] Information obtained from in-pile fuel behavior studies performed at the Idaho National Engineering Laboratory in the Power Burst Facility (PBF) reactor and at the Halden Heavy Boiling Water Reactor, in Norway, provides an experimental data base for assessment of NRC reactor licensing criteria and comparison with calculated fuel rod behavior. The tests are being conducted as part of the Thermal Fuels Behavior Program of EG&G Idaho, Inc., and sponsored by the Nuclear Regulatory Commission's Water Reactor Safety Fuel Behavior Research Program.[2,3]

The purpose of this report is to examine the performance of FRAP-T5 in simulating fuel rod behavior. Emphasis is placed on a qualitative review of the code performance by comparison of in-pile data and postirradiation examination measurements with the code calculations. This is the second in a continuing series of FRAP-T review documents.[4] A brief description of the computer code is presented in Section 2. Section 3 contains discussions of measured fuel rod behavior and comparisons with performance code calculations under steady state conditions; in Section 4, the transient fuel and cladding behavior is discussed. Conclusions concerning the results of this study are summarized in Section 5.

2. CODE DESCRIPTION

The FRAP-T computer code was developed to describe the transient behavior of nuclear fuel rods during hypothesized accident conditions ranging from mild operational transients to design basis accidents such as the loss-of-coolant accidents (LOCAs), power-cooling-mismatch accidents (PCMs), and reactivity initiated accidents (RIAs). The code described in this report is the fifth of a series of fuel rod behavior codes (FRAP-T MOD005; Version FL1130) developed from succeeding versions incorporating advances made in fuel rod modeling and response. Whenever the designation FRAP-T appears, FRAP-T5 is implied, unless otherwise identified.

FRAP-T is a modular code utilizing separate models (or subroutines) for each user-specific type of computation and analysis. The code is restricted to analysis of zircaloy-clad uranium dioxide fuel rods linked to the materials properties subcode MATPRO.[5] FRAP-T iteratively calculates the variation with time of all significant interrelated fuel rod effects, including fuel centerline temperature, cladding temperature, fuel and cladding deformation, fission gas release via the GRASS code[6] and increase in internal gas pressure, thermal expansion of the fuel and cladding, and cladding oxidation.

Coolant boundary conditions required as input by FRAP-T are coolant pressure, inlet temperature, flow and enthalpy histories. These variables may be obtained from the results of a thermal-hydraulic code such as RELAP.[7] No restrictions are placed on the power or coolant boundary conditions of the fuel rods analyzed.

The initial conditions of an unirradiated fuel rod prior to a transient can be determined by FRAP-T. However, for previously irradiated rods, a steady state analysis is required to determine the burnup dependent fuel rod status prior to the initiation of a transient calculation. The FRAPCON-1 computer code has been developed to calculate the steady state operating parameters of irradiated fuel rods required as initial conditions

to FRAP-T.[8] The basis of FRAPCON-1 is the FRAP-S3 code, incorporating the fuel temperature subcode from the GAPCON-THERMAL computer code.[9,10] FRAPCON calculates burnup dependent variables, such as fission gas inventory, fuel densification and swelling, cladding deformation, and fuel-cladding interface pressures and gaps, which are transferred to FRAP-T by restart tape.

The calculational procedure is illustrated in Figure 1, and begins by input data processing. The fuel rod condition at the beginning of the transient is determined through a self initializing (steady state) calculation. The time is advanced according to an input-specified time step, and the fuel rod status at the new time is determined, providing the initial conditions for the next time step. The length of the rod is divided into user-specified axial segments (nodes), each assumed to operate for a single set of conditions over its length for the time step iteration. The fuel rod power history is approximated by incrementing the power levels with instantaneous jumps from one power level to another. Fuel and cladding temperatures, fuel thermal expansion, cladding thermal expansion, and cladding deformation for each axial node are calculated separately. The fuel-cladding deformation is integrated over the length of the fuel rod and added to previous values to obtain the rod internal pressure. The pressure is fed back into the fuel and cladding elastic and plastic deformation calculations during subsequent iterations to evaluate thermal expansion and gas gap width within each axial node. The calculations are cycled until convergence occurs for the time step in the user-specified transient. After the initializing time step, fission gas release is determined after the calculations have converged, and is determined only once per time step. Complete descriptions of the code structure and computational schemes outlined are contained in the references.

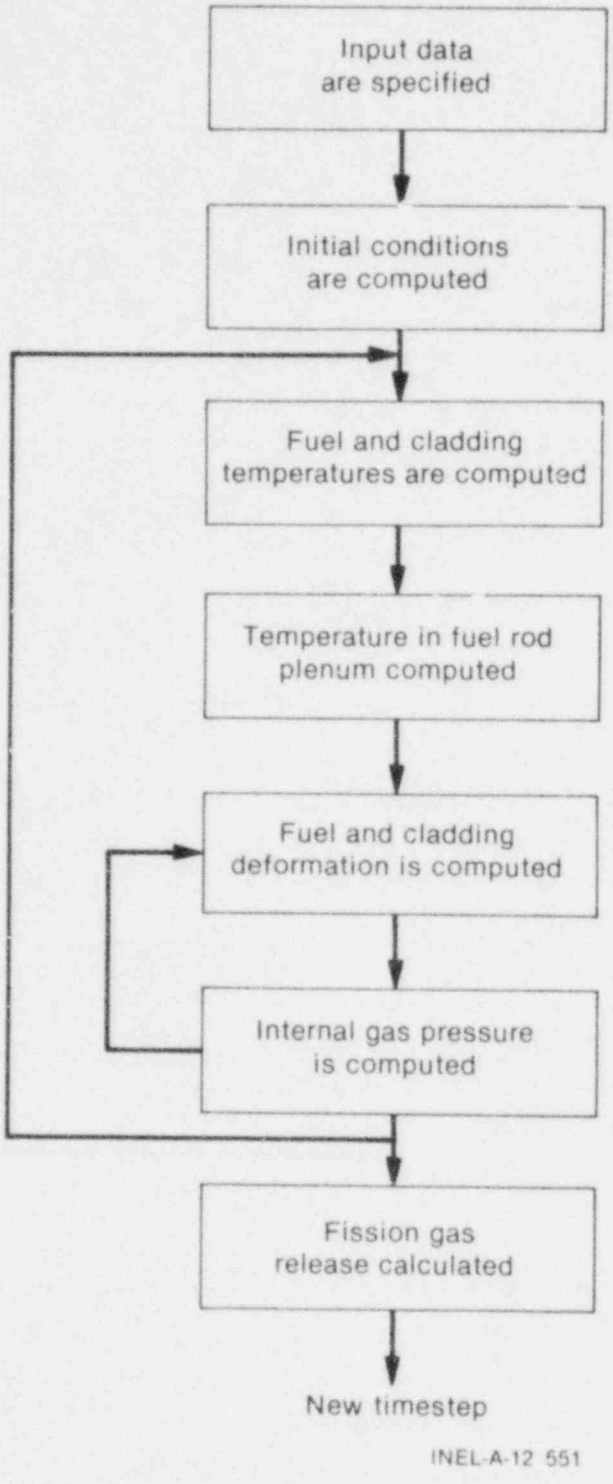

Fig. 1. Simplified FRAP-T5 flow chart of the calculational procedure.

The next version of the FRAP-T code is FRAP-T6, currently under development.[a] The developmental version used in the calculations presented here differs from FRAP-T5 by incorporation of an updated model of gap conductance[b], instead of the modified Ross and Stoute model, and a nonuniform gas gap instead of a uniform annular gap, and is a preliminary version of the FRAP-T6 performance code expected to be issued at a later date.

---

a. FRAP-T6 (MOD6) version 7/9/80 Configuration Control Number H-002483B.

b. Pacific Northwest Laboratories GAPCON-II gap conductance model.[11]

3. FUEL TEMPERATURE UNDER STEADY STATE OPERATION

The gas gap conductance between the fuel and cladding is a major factor in determining the fuel temperature under all operating and transient conditions. Heat transfer from the fuel primarily determines the amount of stored energy in the fuel. Stored energy in the fuel is a controlling factor in the nuclear fuel rod behavior during accident situations.

As part of the U.S. Nuclear Regulatory Commission's Water Reactor Safety Research Fuel Behavior Program, EG&G Idaho, Inc. is conducting fuel rod behavior studies in the Heavy Boiling Water Reactor in Halden, Norway to measure the effects of fuel rod internal pressure and composition on fuel temperature.[12] The Instrumented Fuel Assembly-430 (IFA-430), operated in the Halden Reactor, is a multipurpose assembly designed to provide information about the effect of fill gas pressure and composition on fuel thermal performance, the axial gas flow characteristics of fuel rods, cracking and relocation of the fuel pellets, and the release of fission gases.

This section reviews the fuel rod gap conductance models used in FRAP-T5[a] and a developmental version of FRAP-T6, and compares steady state fuel temperature resulting from changes in the rod internal gas pressure and composition as calculated by FRAP-T5 and FRAP-T6 with data from IFA-430. The IFA-430 data are unique in that the fuel rod fill gas composition and pressure were varied during actual nuclear operation which removes the uncertainty in rod-to-rod variation present in typical tests of this type, and permits a wide variation of pressures and fill gas inventories.

The FRAP-T calculations were carried out using the default deformation model option of the code. The FRACAS-I deformation model (MODFD=2) was

---

a. FRAP-T5 (MOD5) VERSION 7/26/79 Configuration Control Number H-000583B

used which assumes no stress deformation of the fuel (free thermal expansion) and no fuel relocation, one of severed models available in the FRAP-T code. Another model, specifically, the FRACAS-I with cracked fuel thermal conductivity and fuel relocation options (MODFD=3), was used in a preliminary analysis and resulted in calculated fuel centerline tempertures which were less representative of the measured temperatures. Thus, although the physical processes are more appropriately considered in the MODFD= option, this option was not used in the present analysis. Based on general experience, the MODFD=3 option is expected to give better calculated temperatures at higher linear heat ratings (30 to 40 kW/m) than for the low values (<25 kW/m) used in this analysis.[13] The FRAP-T general input data used in the calculation are listed in the Appendix. A single fuel rod calculation was performed using one coolant flow channel and five axial nodes. The gas flow model was not used, and thus instant internal rod pressure equilibrium was assumed. A central void was specified for the problem to account for the fuel centerline thermocouple. Ten radial mesh nodes were used to describe the fuel (7 nodes), gas gap (2 nodes), and cladding (3 nodes) behavior at each axial node.

3.1 Gap Conductance Model

Changes in the pressure and composition of the fuel rod fill gas as a function of burnup affect the gap conductance and fuel temperature. The models used to calculate gap conductance include the effects of increasing pressure and contamination of the helium fill gas with xenon fission gas. The model for the gap conductance used in FRAP-T5 is basically a modification of the formulation due to Ross and Stoute[14] which, for noncontact (fuel-cladding) conditions, assumes the gap between fuel and cladding is axisymmetric and that heat is transferred across the gap by conduction through the gas and by radiation. Thus, in FRAP-T5, the gap conductance, h_g, is given by

$$h_g = \frac{k_g}{t_g + (g_1 + g_2)} + h_r \quad , \qquad (1)$$

where

h_g = gap conductance, $[W/(m^2 \cdot K)]$

k_g = conductivity of gas in gas gap, $[W/(m \cdot K)]$

t_g = gap thickness, (mm)

g_1 = temperature jump distance at cladding inside surface, (mm)

g_2 = temperature jump distance at fuel outside surface, (mm)

h_r = radiant heat transfer conductance, $[W/(m^2 \cdot K)]$.

The radiant heat transfer coefficient is computed using the following equation

$$h_r = \sigma F_e (T_f^2 + T_c^2)(T_f + T_c) \quad , \qquad (2)$$

where

σ = Stefan-Boltzmann constant, $[W/(m^2 \cdot K^4)]$

F_e = emissivity factor, (dimensionless)

T_f = temperature of outside surface of fuel, (K)

T_c = temperature of inside surface of cladding, (K).

The emissivity factor is computed by the equation

$$F_e = \frac{1}{e_f} + \frac{r_f}{r_c}\left(\frac{1}{e_c} - 1\right)^{-1} \quad , \tag{3}$$

where

e_f = emissivity of fuel surface

e_c = emissivity of cladding inside surface

r_f = outside radius of fuel, (mm)

r_c = inside radius of cladding, (mm).

The temperature jump distance $(g_1 + g_2)$ is computed by an empirically derived equation in the GAPCON-THERMAL-1[10] code

$$g_1 + g_2 = 5.448 \frac{\mu}{p}\left(\frac{T}{M}\right)^{1/2} \quad , \tag{4}$$

where

μ = viscosity of gas in the fuel-cladding gap [(kg/(m•s)]

P = pressure of gas in the fuel-cladding gap, (MPa)

T = temperature of gas in the gap, (K)

M = molecular weight of gas in the fuel-cladding gap, (kg).

The gap conductance model used in FRAP-T6 is taken from the GAPCON-THERMAL-2[11] code. The gas conductance and temperature jump distance terms and the assumed pellet location within the cladding differ from those used in FRAP-T5. The gap conductance in FRAP-T6 is

$$h_g = \frac{k_g}{t_g + 1.8\,(g_1 + g_2)} + h_r \quad , \tag{5}$$

thus differing from the FRAP-T5 (Equation 1) model by a coefficient of 1.8 in the temperature jump distance.

The thermal jump distance model used in FRAP-T6 is taken from GAPCON-THERMAL-2 and is given by

$$g_i = \frac{k_g\, C}{\sum_j \left(\frac{a_j\, P_j}{M_j\, T_i}\right)} \quad i = 1, 2;\ j = 1 \ldots N \quad , \tag{6}$$

where C is a constant dependent upon the units of k_g, P_j is the partial pressure of the j^{th} gas component N, M_j is the molecular weight of the j^{th} gas component N, a_j the accommodation coefficient (a function of temperature), and T_i the temperature at the gas-solid interface (before temperature jump). For a mixture of helium and xenon gases, the accommodation coefficient is

$$a_i = (a_{Xe} - a_{He}) \left[\frac{M_j - 4}{128}\right] + a_{He} \quad , \tag{7}$$

where the component gas coefficients are

$$a_{Xe} = 0.425 - (2.3 \times 10^{-4})\, T \quad , \tag{8}$$

and

$$a_{He} = 0.749 - (2.5 \times 10^{-4})\, T \quad . \tag{9}$$

The gap conductance calculated with FRAP-T5 assumes the pellet is located axisymmetrically within the cladding. The FRAP-T6 model assumes the pellet is located one-half the fabricated gap size off-center within

the cladding and calculates the average gap conductance for the non-uniform gap. The pellet and gap are divided into three pie shaped segments, the gap conductance is computed for each segment, based on the average gap size in each section, and the gap conductance of the three segments is averaged to give an average gap conductance which is used in the fuel temperature calculations.

In both the FRAP-T5 and FRAP-T6 models, the conductivity of a mixed gas is given by[15]

$$k_{mix} = \sum_{i=1}^{N} \left[\frac{k_i}{1 + \sum_{\substack{j=1 \\ j \neq i}}^{N} \Psi_{ij} \left(\frac{x_j}{x_i} \right)} \right] \tag{10}$$

where the coefficient Ψ_{ij} is

$$\Psi_{ij} = \Phi_{ij} \left[1 + 2.41 \frac{(M_i - M_j)(M_i - 0.142\, M_j)}{(M_i + M_j)^2} \right], \tag{11}$$

with

$$\Phi_{ij} = \frac{\left[1 + \left(\frac{k_i}{k_j} \right)^{1/2} \left(\frac{M_i}{M_j} \right)^{1/4} \right]^2}{2^{3/2} \left(1 + \frac{M_i}{M_j} \right)^{1/2}} \tag{12}$$

and

N = number of components in mixture

$M_{i,j}$ = molecular weight of the i^{th} and j^{th} chemical species

$x_{i,j}$ = mole fraction of the i^{th} and j^{th} chemical species

$k_{i,j}$ = thermal conductivity of the i^{th} and j^{th} chemical species

with $i \neq j$.

The thermal conductivity equations of the individual rare gases are based on the correlative work of Gandhi and Saxena.[16] The resulting expressions are

$$k_{helium} = 3.366 \times 10^{-3} T^{0.668} \quad (13)$$

$$k_{argon} = 3.421 \times 10^{-4} T^{0.872} \quad (14)$$

$$k_{xenon} = 4.0288 \times 10^{-5} T^{0.872} \quad (15)$$

$$k_{krypton} = 4.726 \times 10^{-5} T^{0.923} . \quad (16)$$

3.2 Comparison With Test Data

The FRAP-T calculated fuel temperature response is compared in this section to the measured effects of first, adding up to 10% xenon to the helium fill gas and, second increasing the fill gas pressure from 0.1 to 5.1 MPa.

The IFA-430 test assembly contained four, 1.28-m-long fuel rods loaded with 10% enriched UO_2 pellet fuel.[17] The two rods used in the fill gas

pressure and composition tests, termed gas flow rods, were each instrumented with a centerline thermocouple and three axially spaced pressure sensors. These two rods had a fabricated diametral gap size of 0.10 mm and 0.23 mm, and were connected to an out-of-pile gas supply system. The other two rods, prepressurized with 0.48 MPa of He, were not connected to the gas supply system and were not used in the fill gas pressure and composition tests.

The out-of-pile gas supply system permitted the fill gas composition and pressure to be changed while the fuel rods were operating in-pile. Both pressure and xenon concentration were systematically changed in the rods during the experiment. The fuel centerline temperatures were measured for fill gas pressures ranging from 0.1 to 5.1 MPa and xenon concentrations from 0 to 10%, at rod linear powers from 5 to 25 kW/m. The fuel had a burnup of ∿3 GWd/tU at the time of the experiments and was in a cracked, but stable, condition.

3.2.1 Xenon Effects on Fuel Temperature

The effect of the addition of Xe to the He fill gas is to reduce the gap conductance and fuel effective thermal conductivity. Figure 2 shows the gap conductance as a function of gap size for 100% He and 90% He/10% Xe fill gas at 1.0 MPa, as computed with FRAP-T5 and -T6 for the 0.10 mm gap rod. Qualitatively, the gap conductance calculated by FRAP-T6 increases at a faster rate than that calculated by FRAP-T5 as the gap closes and is higher than that calculated by FRAP-T5 for radial gaps less than ∿0.110 mm.

The 0.23 mm gap rod centerline temperatures calculated with FRAP-T5 and -T6 are compared with the measured centerline temperatures in Figures 3 and 4. In general, the FRAP calculated temperatures were a few percent higher than the measured temperatures, and the FRAP-T6 experimental code calculations were closer to the data than FRAP-T5. Figure 5 shows the measured and FRAP-T5 calculated fuel centerline temperatures for the 0.10 mm gap rod (FRAP-T6 calculated data were not available for this rod);

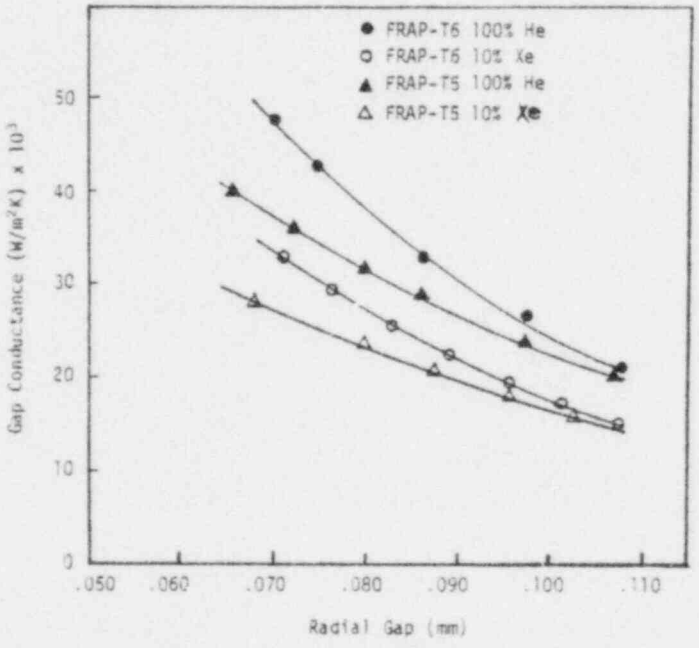

Fig. 2. FRAP-T5 and -T6 calculated gap conductance as a function of radial gap size for 1.0 MPa fill gas pressure and 0.115 mm fabricated radial gap width.

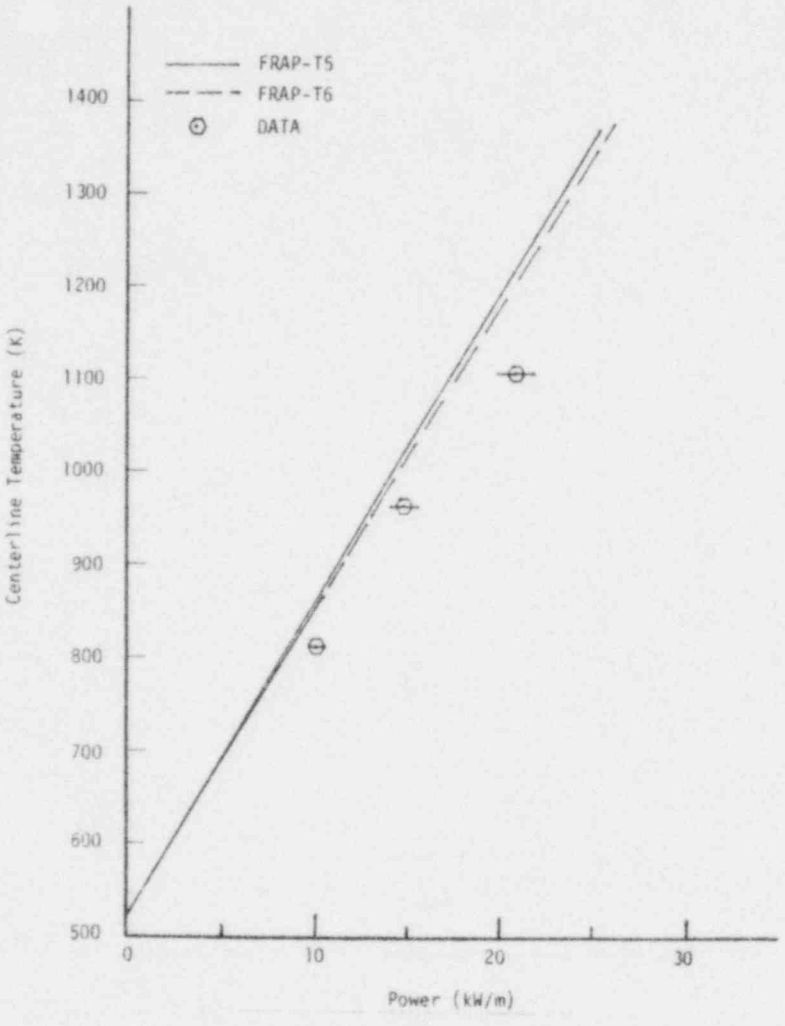

Fig. 3. FRAP-T5 and -T6 calculated centerline temperatures compared with data for 10% Xe fill gas at 1.0 MPa in the 0.23 mm diametral-gap rod.

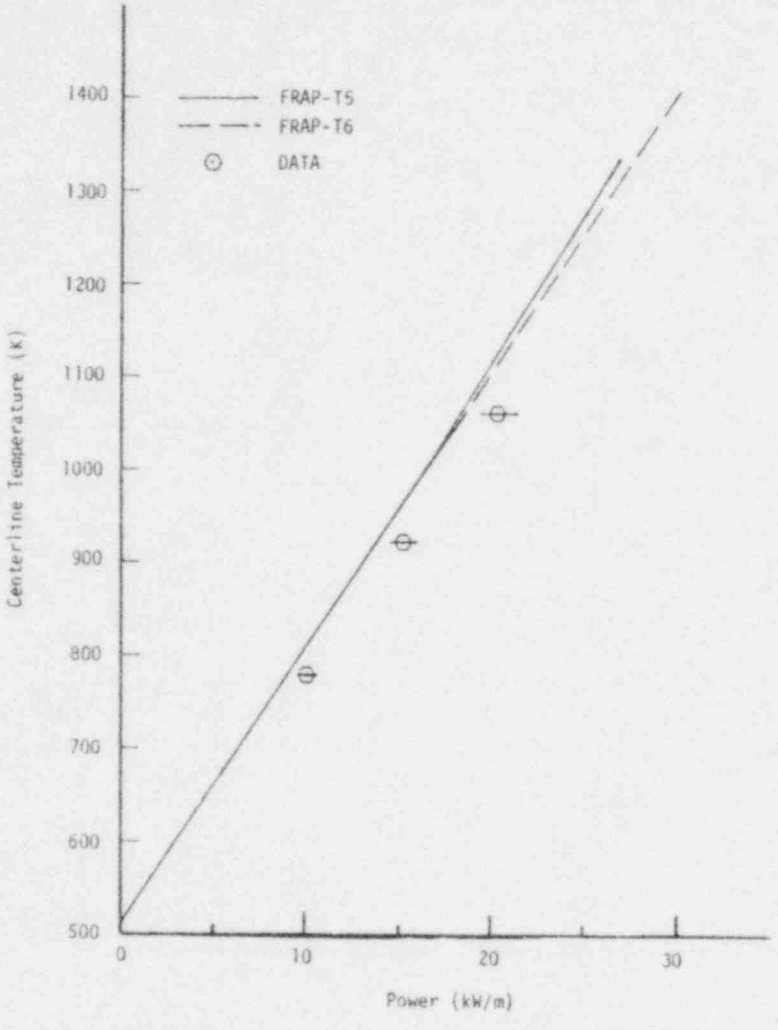

Fig. 4. FRAP-T5 and -T6 calculated fuel centerline temperatures compared with data for 100% He fill gas at 1.0 MPa in the 0.23 mm diametral-gap rod.

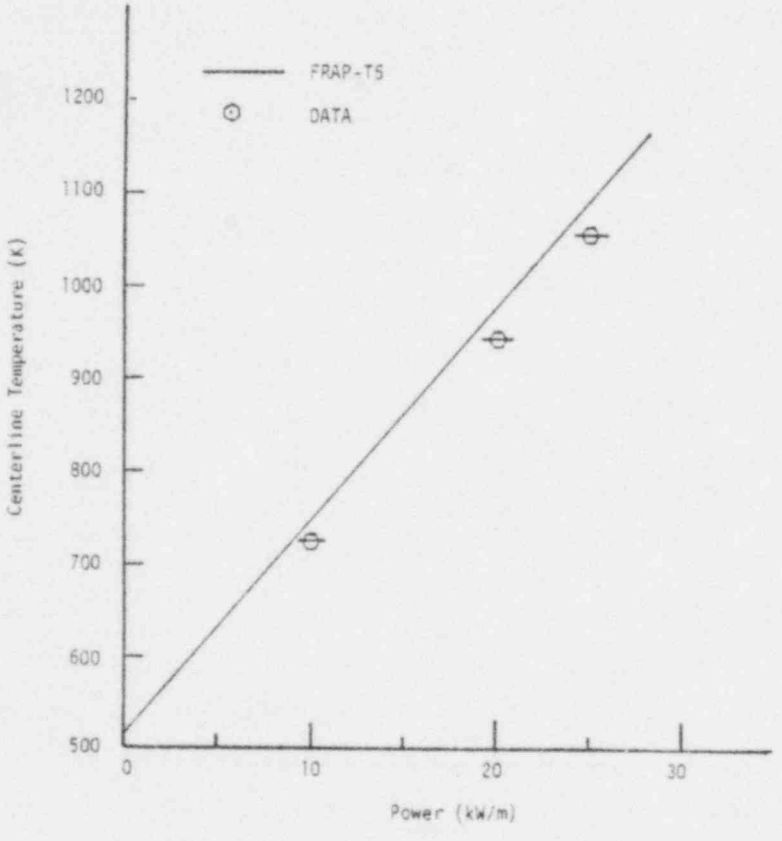

Fig. 5. FRAP-T5 calculated fuel centerline temperature and data for 10% Xe fill gas at 1.0 MPa in the 0.10 mm diametral-gap rod.

the trend shown is the same for the 0.23 mm gap rod. In Figures 6 and 7 the centerline temperature at 10 and 20 kW/m is plotted as a function of percent Xe in the fill gas. The FRAP-T calculations diverge from the data by overcalculating the fuel centerline temperatures as the xenon concentration increases. The increase in centerline temperature from that measured with 100% He fill gas is plotted as a function of the percent Xe in the fill gas in Figure 8. The FRAP-T calculated temperatures are higher than the data, as shown earlier, and diverge from the measured data. The FRAP-T6 model predicts temperatures closer to the measured temperatures than FRAP-T5. Such results suggest that the method of calculation chosen for the FRAP-T5 analysis may not correctly take into account the effective fuel thermal conductivity. The options chosen for this analysis allow only changes in the gap thermal conductance. The divergence between the measured and calculated temperatures indicates that the FRAP-T results should be used with caution at high Xe concentrations until further data are available.

3.2.2 Pressure Effects on Fuel Temperature

The pressure influences the fuel centerline temperature through the temperature jump distance contribution to the fuel-cladding gap conductance, as shown in Equations (1), (4) and (6). The measured centerline temperature change as a function of pressure is compared in Figure 9 with the FRAP-T5 calculated change for the 0.1 mm gap rod. The FRAP-T5 results generally agree with the data for both the 100% He and 10% Xe/90% He cases; however, the calculated decrease in fuel centerline temperature with pressure for 100% He is slightly greater than the data. The FRAP-T5 calculated and measured temperature change data are presented in Figure 10 for the 0.23 mm gap rod at 20 kW/m with 100% He and 95% He/5% Xe fill gas; the FRAP-T5 calculations agree very well with the data. In the case of the 0.23 mm gap with 10% Xe fill gas, however, the FRAP-T5 and -T6 calculated temperature change does not follow the data trend at pressures above 2.0 MPa as shown in Figure 11.

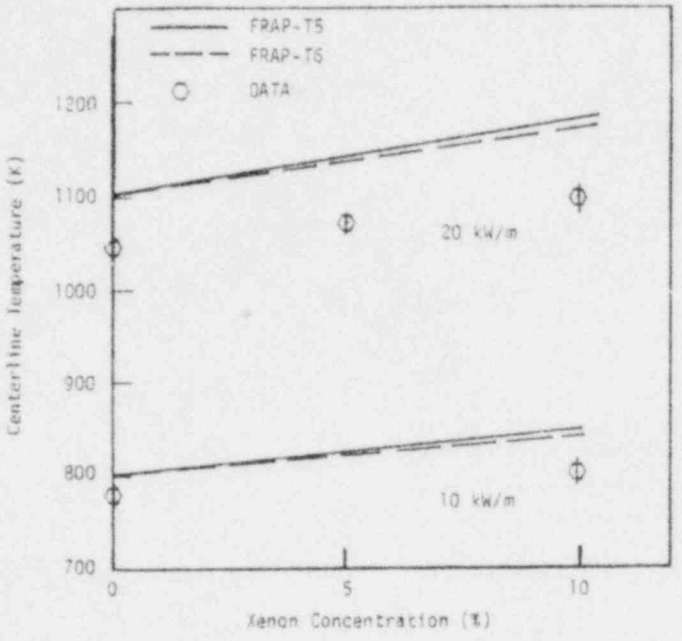

Fig. 6. Measured and FRAP-T5 and -T6 calculated fuel centerline temperatures as a function of Xe concentration in the fill gas for the 0.23 mm diametral-gap rod at 1.0 MPa pressure.

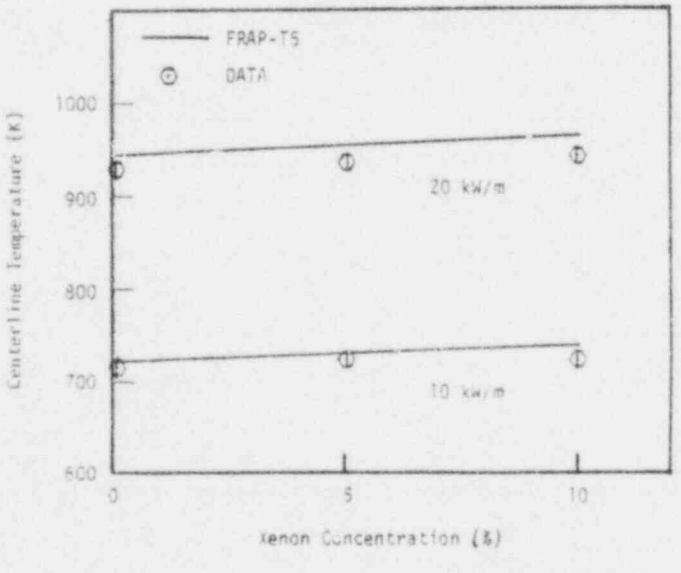

Fig. 7. Measured and FRAP-T5 calculated fuel centerline temperature as a function of Xe concentration in the fill gas at a pressure of 1.0 MPa (0.10 mm diametral gap).

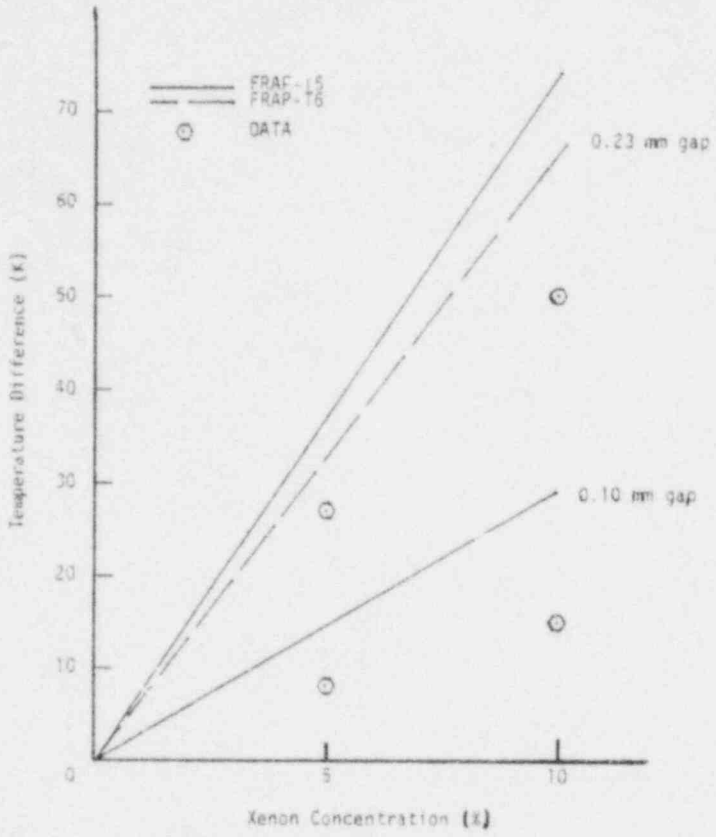

Fig. 8. Measured and FRAP-T5 calculated temperature change due to increasing xenon concentration for the 0.10 and 0.23-mm diametral-gap rods.

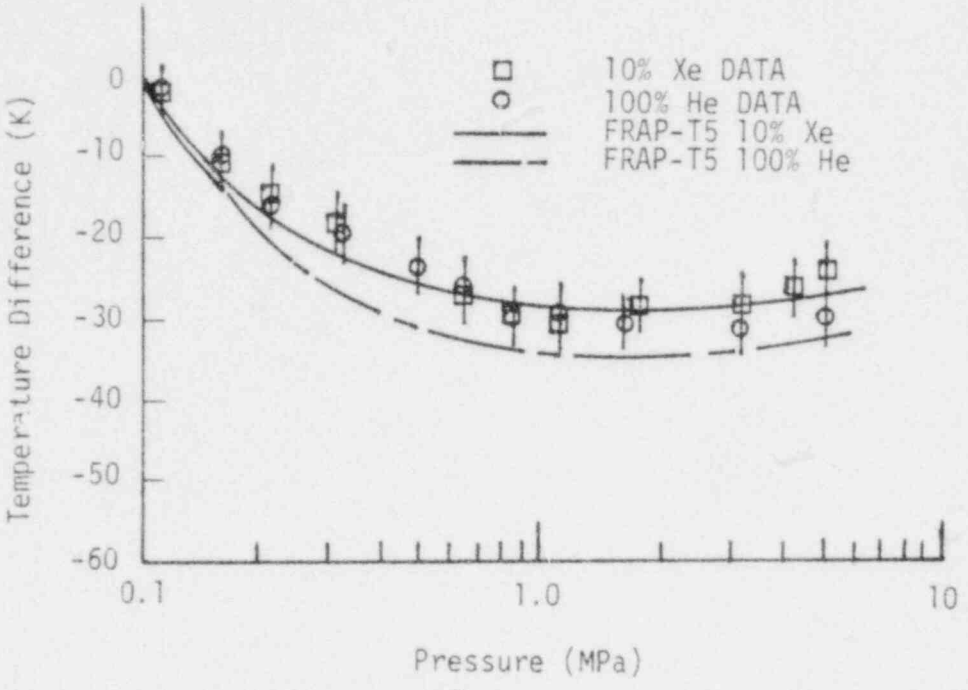

Fig. 9. Measured and FRAP-T5 calculated centerline temperature change as a function of fill gas pressure with 100% He and 10% Xe/90% He fill gas in the 0.1 mm diametral-gap rod.

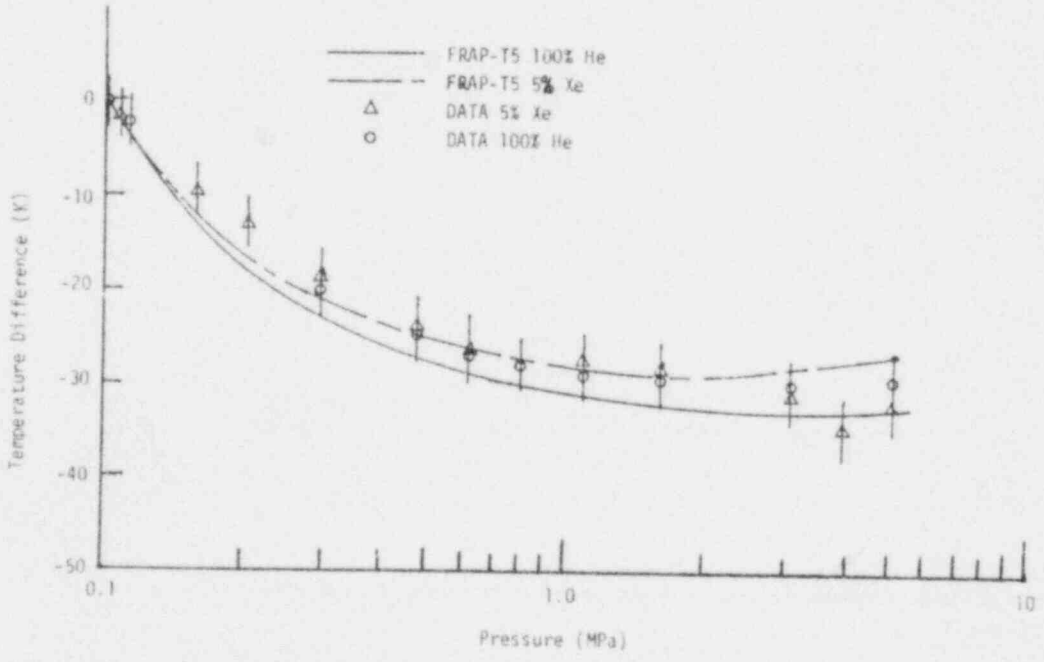

Fig. 10. Measured and FRAP-T5 calculated centerline temperature change due to increasing fill gas pressure for the 0.23 mm diametral-gap rod.

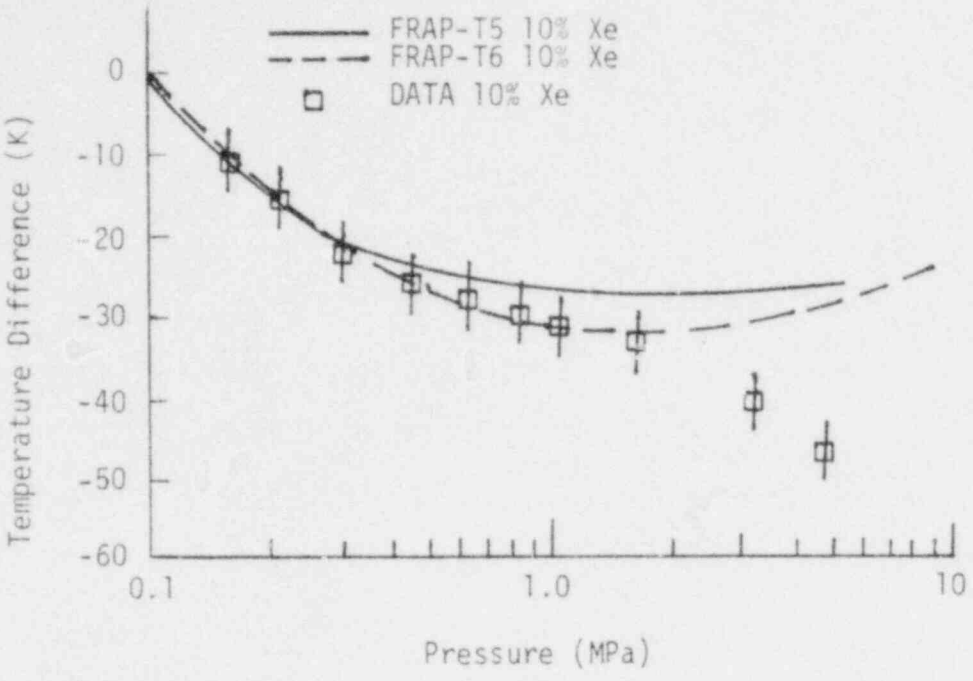

Fig. 11. Temperature difference data versus pressure for 10, 15, and 20 kW/m with 10% Xe in the 0.23 mm diametral-gap rod.

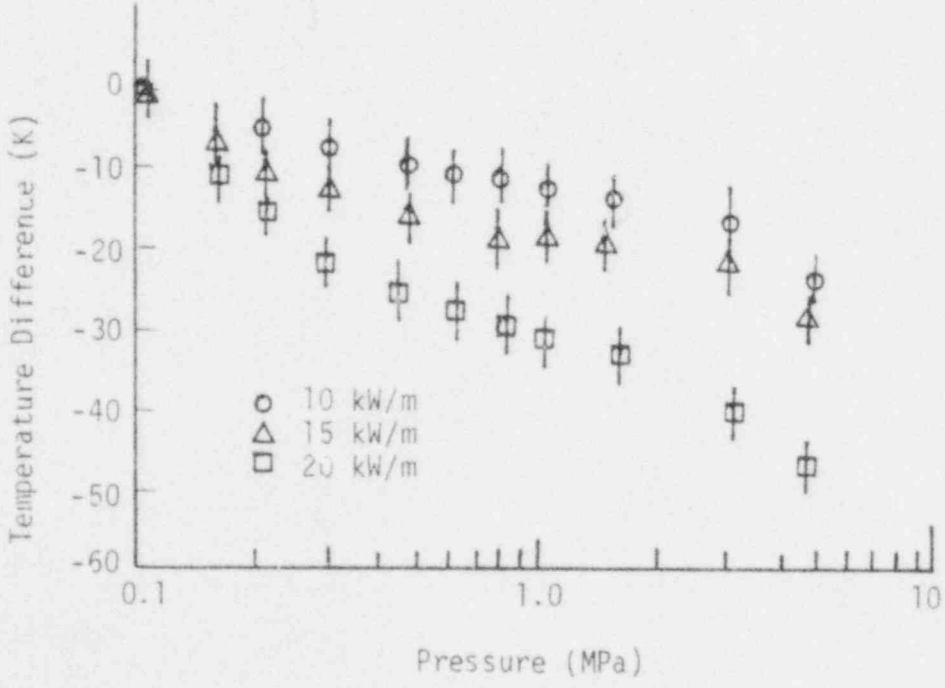

Fig. 12. Measured change in fuel centerline temperature as a function of fill gas pressure for 10% Xe in the 0.23 mm diametral-gap rod.

The measured temperature drop data at 10, 15, and 20 kW/m powers for the 0.23 mm gap rod with 10% Xe/90% He fill gas, shown in Figure 12 further illustrates the unexpected decreases in temperatures at pressures above 2.0 MPa. The downward trend in the data at pressures above 2.0 MPa is not presently understood. The contribution of the Xe temperature jump distance to the gap conductance is only 1-2% and is not expected to produce the discrepancy between the calculated and experimental results observed here. However, in terms of the integral behavior, pressure effects on the thermal jump distance (see Equations 4, 5, and 6),[18] may also be significant in the fuel cracks. Such effects on the effective thermal conductivity are not modeled in the option used for these calculations, and should be taken into consideration to adequately assess the FRAP-T performance.

In summary the effects of increased fill gas pressure are: (1) to decrease fuel temperatures (enhance rod conductivity) in the range 0.1 to 2.0 MPa for which FRAP-T calculations agree very well; (2) insignificant in the range 2.0 to 5.0 MPa for the 0.10 mm gap rod at Xe concentrations less than 10%, and for the 0.23 mm gap rod at Xe concentrations less than 5%, again for which FRAP-T calculations agree; and (3) to unexpectedly decrease fuel temperatures in the range 2.0 to 5.0 MPa in the 0.23 mm gap rod at a Xe concentration of 10%, a trend not calculated by the FRAP-T options used for this analysis.

3.3 Conclusions Regarding Steady State Fuel Temperature Calculations

The measured effects of fuel rod fill gas composition and pressure on the steady state fuel temperature when compared with the FRAP-T code show:

1. The FRAP-T calculated fuel centerline temperature is 3 to 7% higher than the measured temperature, but within the experimental error, for a range of xenon concentrations of 0 to 10% (in helium) of the fill gas. However, the FRAP-T calculated centerline temperature as a function of xenon concentration in the fill gas diverged from the measured temperatures, indicating that other models in the performance code should be considered in the FRAP-T calculations at higher xenon concentrations.

2. FRAP-T adequately models the effect of fill gas pressure on fuel temperature in the range 0.1 to 5.0 MPa for fill gas compositions ranging from pure helium to helium with 10% xenon in fuel rods with 0.1 and 0.23 mm fuel-cladding gap sizes with one exception. For the combination of the 0.23 mm gap with >5% xenon in the fill gas, at pressures up to 2.0 MPa the FRAP-T calculations follow the data reasonably well. However, above 2.0 MPa the fuel behavior unexpectedly changed and the FRAP-T calculations which utilize limited models could not be expected to follow this data trend.

4. TRANSIENT FUEL AND CLADDING BEHAVIOR

Transient test data chosen for comparison with the computer code calculations are from the RIA test program. EG&G Idaho, Inc., has conducted RIA irradiation tests in the PBF reactor as part of the NRC Water Reactor Safety Fuel Behavior Research Program, to investigate fuel damage and failure mechanisms over a broad range of fuel enthalpies.[19] Twelve fuel rods have been tested in six separate tests with radial-average peak fuel enthalpies ranging from 185 to 350 cal/g UO_2. The results of these tests are summarized in Table 1. The test fuel rod assemblies and test rods were selectively instrumented for measurement of coolant temperature and flow conditions, shroud pressure, cladding elongation, rod internal pressure, fuel centerline temperature, plenum gas temperature, cladding surface temperature, and the instantaneous and integrated relative neutron flux profile. In the following discussions, measured and calculated thermal and mechanical responses of test rods to hypothesized RIA conditions are presented, to evaluate the capability of the FRAP-T5 computer code to predict transient fuel and cladding behavior and to characterize the sequence of fuel rod damage events during the transient.

4.1 Fuel Thermal Response During an RIA

Representative calculations of fuel temperature distributions were performed with the FRAP-T5 computer code[1,a] using Test RIA 1-1 fuel rod and experimental data to assess test rod thermal boundary conditions relevant to RIA fuel behavior.

The Test RIA 1-1 fuel rods were subjected to a single power burst of about 50 ms duration with initial coolant conditions of 538 K, 6.45 MPa, and 0.085 L/s per rod. The large power burst produced rapid fuel rod failure, as indicated by on-line instrumentation data. The fission product

---

a. FRAP-T5, Version FL1130, Idaho National Engineering Laboratory, Configuration Control Number H003891B was used for the analyses presented in this report.

TABLE 1. PBF-RIA TEST RESULTS

RIA Test	Fuel Rod Type	Fuel Enrichment ($\%^{235}$ U)	Burnup (Mwd/t)	Radial Power Peaking Factor	Radial-Average Total Energy Deposition[a] (cal/g UO_2)	Radial-Average Peak Fuel Enthalpy[b] (cal/g UO_2)	Peak Local Fuel Enthalpy[c] (cal/g UO_2)	Comments
RIA ST-1 Burst 1	17 x 17 PWR	5.8	0	1.076	250	185	205	Did not fail; first test on ST-1 rod
RIA ST-1 Burst 2	17 x 17 PWR	5.8	0	1.076	330	250	275	10% fuel washed out; second test on ST-1 rod
RIA ST-2	17 x 17 PWR	5.8	0	1.076	345	260	290	15% fuel washed out
RIA ST-3	17 x 17 PWR	5.8	0	1.076	300	225	250	Did not fail
RIA ST-4	15 x 15 PWR	20.0	0	1.48	695	350[d]	530[d]	Completely destroyed; 35 MPa pressure pulse measured
RIA 1-1	2-Saxton	5.7	4600	1.13	365	285	330	Complete shroud flow blockage
	2-Saxton	5.8	0	1.077	365	285	315	Severe Failure - partial flow blockage
RIA 1-2	4-Saxton	5.7	5000	1.13	240	185	215	One rod failed - three rods did not fail

a. Five methods were used to measure the test rod radial average fission energy deposited during each transient.[20] Detailed independent review of the five measurement methods confirmed that none were unreliable. The five measurement methods had estimated uncertainties ranging from +11 to +14%. These are conservative estimates of the uncertainties and based on previous PBF results (where the average burnup measurement is within 3% of the average thermal-hydraulic power measurement), these results are considered accurate to within about +6%.

b. The FRAP-T5 computer code[1] was used to determine the axial peak radial average fuel enthalpy from the measured total energy deposition. The fraction of energy generated by delayed neutrons after control rod scram was calculated using the TWIGL computer code (Configuration Control Number H0099718). TWIGL solves the coupled time and space-dependent neutron diffusion and thermal-hydraulic equations for a reactor in two dimensions.

c. This value will vary somewhat depending on the node sizes in the analytical models used to convert total energy deposition to peak local fuel enthalpy.

d. Fuel enthalpy at time of failure, approximately 3 ms after the time of peak power.

detection system and the loop system radiation monitor indicated rod failure several minutes after the power burst, due to the time delay in fission product transport to these instruments. The best estimate of the total energy deposition was an approximate total fuel pellet radially averaged adiabatic energy of 365 cal/g UO_2 at the axial peak power, corresponding to a radial average peak fuel enthalpy of 285 cal/g. Roughly 80% of the total adiabatic energy was deposited in the fuel rod by the time of reactor shutdown.

The FRAP-T5 computer code was used to calculate the peak fuel enthalpies for Test RIA 1-1, and account for heat transfer from the fuel to the cladding and reactor coolant during the RIA power transient. Since gap closure occurred prior to the time of peak power, gap conductance uncertainties are minimal. The best estimate of the measured energy deposition was input to the FRAP-T5 computer code. One previously irradiated rod and one fresh, unirradiated rod, enclosed in a single coolant flow channel were analyzed.[21] Transient coolant conditions were determined using the W-3 heat flux correlation and the Groeneveld equation to descibe the post-critical heat flux (CHF) heat transfer. The FRACAS-I fuel deformation model was used, with an option which assumes fuel relocation but no stress deformation of the fuel. Twelve axial and 14 radial mesh nodes were used to characterize the fuel rod. The general FRAP-T input data used in the RIA calculation are listed in the Appendix.

Coolant conditions for Test RIA 1-1 used in the FRAP-T calculations were calculated using the RELAP4/MOD5 computer code.[7,a] RELAP4 models system fluid conditions including flow, pressure, mass inventory, fluid quality, and heat transfer. The heat flux through the cladding during steady state operation was obtained from the approximately constant volumetric heating. Almost all of the nuclear heat generated during

---

a. RELAP4/MOD5, Idaho National Engineering Laboratory, Configuration Control Number H0030018.

the RIA, including a prompt gamma-ray contribution, went into increasing the fuel temperature during the power burst. The fuel peak temperature is thus reached quite early in the transient, near the time of reactor scram. The maximum energy deposition during an RIA occurs near the fuel pellet surface due to self-shielding. The radial heat flow is a function of the pellet radius and must be solved numerically. The thermal energy that produces rod damage was assessed in the computer calculations by assuming approximate adiabatic heating in the fuel during the power burst, and equating the burst energy deposition to the fuel rod enthalpy increase.

The results of the FRAP-T5 fuel behavior computations for the previously irradiated rod in Test RIA 1-1 indicated that fuel melting ($T > 3098$ K) occurred at the axial power peak within 6 ms after the time of peak power at a peak fuel enthalpy of 237 cal/g.[a] Peak power occurred about 37 ms after the initiation of the power burst. Melting temperatures appeared first within an annulus near the pellet surface from 0.93 to 0.97 r_o (r_o = pellet radius) due to self shielding, and then spread across the pellet to the center to form a cylindrical region of molten fuel in the peak power region, during the next 8 ms, before decreasing temperatures occurred near the surface. A surface peak temperature of 2020 K was indicated by the calculation at the fuel surface node (at 0.99 r_o) when the maximum extent of fuel melting was reached. Thus, FRAP-T5 predicts no melting at the surface of the fuel pellets. This radial, time-dependent temperature behavior of the fuel is illustrated in Figure 13 for the axial peak power location.

By the time the maximum peak fuel enthalpy was calculated to occur, about 24 ms after the time of peak power, fuel melting began to shift away from the pellet surface region to the interior of the fuel pellet due to heat flow out of the fuel to the cladding and coolant. The radial peak temperature (3098 K) at the fuel centerline occurred at about the time of peak fuel enthalpy, and remained near the melting temperature until the rod began to cool by transfer of stored heat to the coolant. The shifting of

---

a. Radially averaged peak local fuel enthalpy of 268 cal/g.[20]

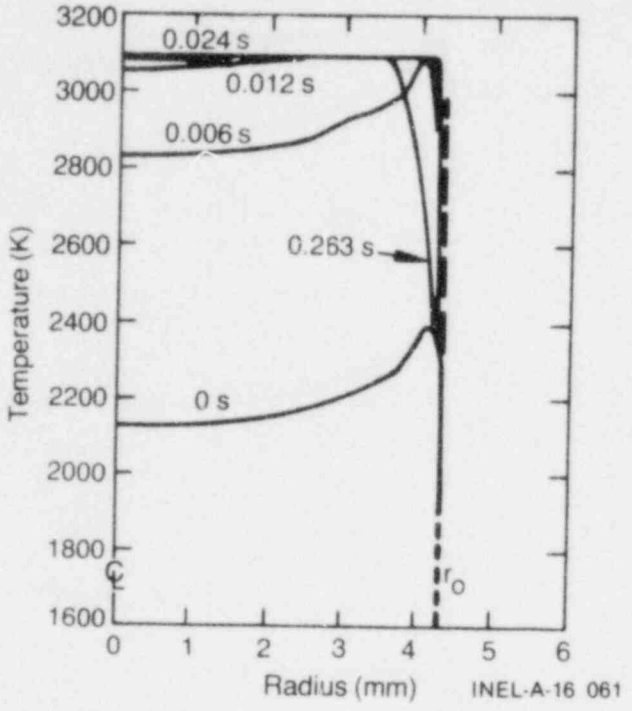

Fig. 13. Calculated fuel radial temperature profiles for several times at the peak power elevation (0.43 m), after the time of peak power.

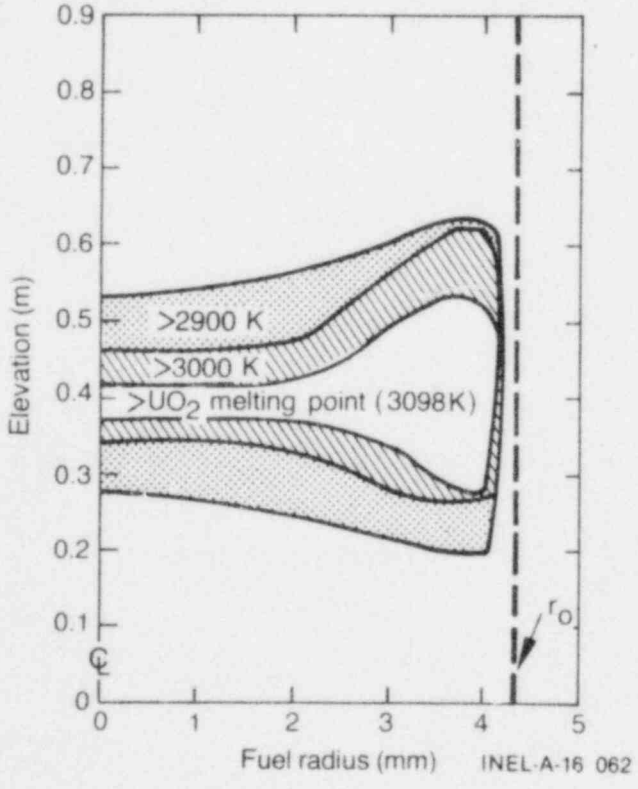

Fig. 14. Calculated fuel temperature map for Rod 801-1 at the time of peak fuel enthalpy during Test RIA 1-1.

high fuel temperatur[illegible] to the interior of the fuel pellet produced a very steep temperature gradient between the molten interior (T = 3098 K) and the surface of the fuel pellet (T = 1857 K at the fuel surface node, 0.99 r_o), as seen in Figure 13. The maximum axial extent (volume) of molten fuel calculated was limited, as illustrated in Figure 14, and extended between 0.275 and 0.53 m (axial nodes) on the rod at the time of peak fuel enthalpy. Fuel melting up to about 22 vol% of the 0.914-m-long fuel stack was estimated from the FRAP-T calculations, with over half of the melting being within the axial region of peak power. The typical parabolic radial temperature profile was reestablished in the fuel about 1 s after the time of peak power (~76 ms after reactor scram). The radial temperature history of the previously unirradiated rods was similar to that calculated for the previously irradiated rod, except that the radial fuel temperature profile of the previously irradiated rod exhibited a steeper thermal gradient near the pellet surface than that for the fresh rod. These results are due to a 10% higher radial power peaking factor in the previously irradiated rods from plutonium produced during long-term irradiation. The calculated temperature histories emphasize that energy deposition near the outer pellet surface region has a dominant effect in determining the heat flux out of the fuel during the early portion of the RIA transient and, thus, in determining the maximum cladding temperatures achieved during the transient.

4.1.1 Fuel Centerline Temperature

The calculated transient fuel centerline temperature was compared with the measured value resulting from the transient for one of the previously unirradiated rods. Rod 801-3 used in Test RIA 1-1 was instrumented with a tungsten-rhenium centerline thermocouple. The thermocouple junction was positioned 0.79 m from the bottom of the fuel stack, at the same elevation as the 180-degree surface thermocouple junction.

The response of the centerline thermocouple to fuel heating during and following the test power burst is plotted in Figure 15. The measured fuel

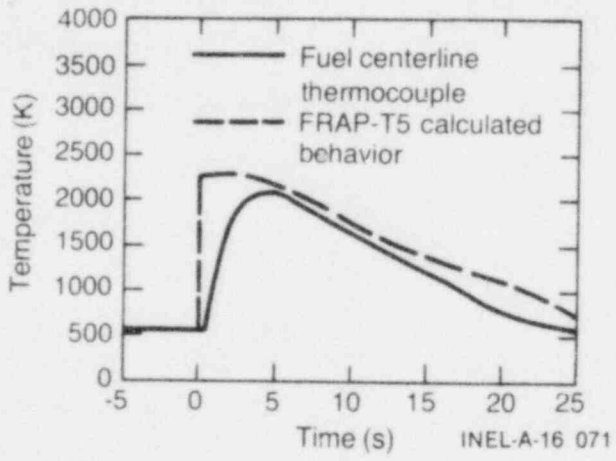

Fig. 15. Comparison of the measured thermocouple response of previously unirradiated Rod 801-3 following the Test RIA 1-1 power burst and the calculated fuel centerline temperatures.

centerline temperature reached 2170 K about 4 s after the time of peak power. FRAP-T5 calculated a maximum fuel centerline temperature at 0.79 m of 2333 K at 2 s after the time of peak power. Thus the thermocouple reading appears to lag behind the rapid temperature increase calculated by FRAP -T5. The time lag is attributed to delayed response of the junction to fuel temperature changes, coupled with poor radial heat transfer across the gap from the fuel to the thermocouple, which can account for the roughly 7% discrepancy noted between the measured and the calculated centerline peak temperatures at this elevation.[22] The calculated centerline peak temperatures thus appear to be in good agreement with the measured temperatures.

4.1.2 Fuel Melting Behavior

Stoichiometric $UO_{2.0}$ melts congruently at about 3100 K, with the liquid and solid in equilibrium at the same composition,[23] as shown by the partial phase diagram for UO_{2+x} presented in Figure 16. Nonstoichiometric UO_{2+x} behaves differently upon melting, with melting beginning at lower temperatures than for UO_2. The melting proceeds gradually, with liquid and solid of different compositions in equilibrium. The latent heat of fusion is absorbed over a range of temperatures, which depends on the overall composition. These observations indicate that previously irradiated uranium dioxide fuel, which is expected to be slightly hyperstoichiometric ($UO_{2+x} \approx UO_{2.01}$ at about half an atomic percent burnup for the Test RIA 1-1 fuel), would be expected to begin melting at lower temperatures (~3080 K) than fresh, stoichiometric fuel (~3100 K). The threshold energy to induce melting, therefore, would be expected to be slightly less (~3 cal/g) for previously irradiated UO_2 than for fresh fuel, a condition not predicted by FRAP-T which uses only the melting temperature of stoichiometric UO_2. More molten fuel was observed in the previously irradiated fuel rods than the fresh fuel rods.

Fuel melting predicted by FRAP-T5 during Test RIA 1-1 began near the pellet surface and progressed radially outward and inward due to heat conduction in the fuel. The time dependence of fuel pellet radial

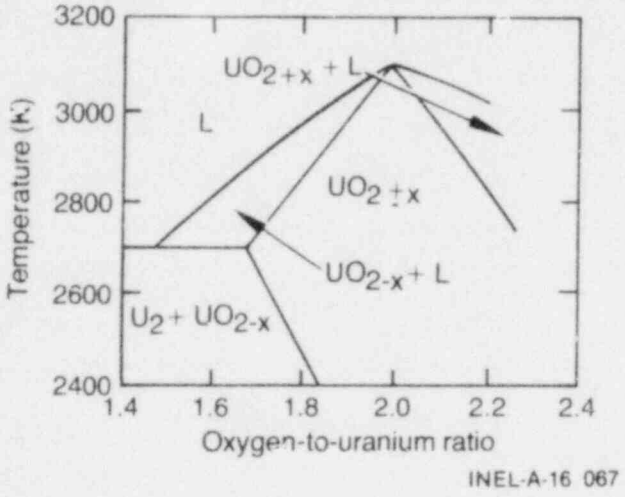

Fig. 16. Partial phase diagram for urania, between $UO_{1.4}$ and $UO_{2.23}$.

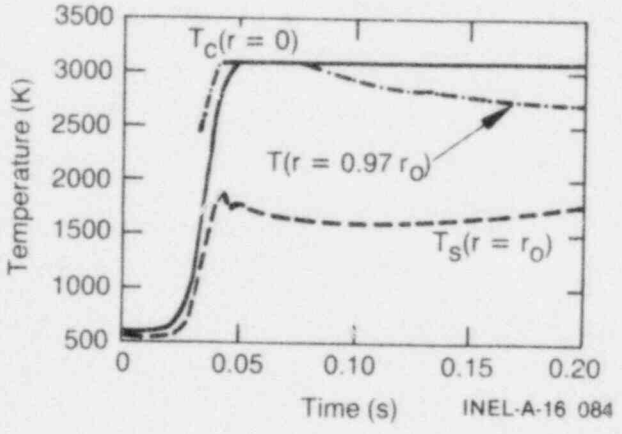

Fig. 17. Fuel temperatures calculated by FRAP-T5 at the axial peak power location as a function of time for several radial positions in the fuel.

temperatures at the axial peak power elevation is plotted in Figure 17 for several radial nodes, as determined by FRAP-T5. The FRAP-T5 code calculated incipient fuel melting as an annulus at an enthalpy of 237 cal/g UO_2, 6 ms after the time of peak power. The calculated fuel melting then extended radially into the center of the fuel, forming a solid cylinder of molten UO_2, but melting temperatures were not predicted at the pellet surface. However, fuel melting at the centerline was not observed metallographically. A more accurate representation of the actual fuel melting determined from the postirradiation examination of fuel from Test RIA 1-1 is that of an annulus of molten fuel between two regions of solid fuel, illustrated schematically in Figure 18, which widens locally about the radial position that first liquified. The reasons for such differences between calculated and measured results is not precisely known, as for example, whether inadequate thermal boundary conditions were used as input to the code, or fuel melting for such a rapid transient is not correctly modeled in the FRAP-T code.

The difficulty in identifying evidence of molten fuel in the RIA 1-1 pellets is illustrated by examples from the metallographic examination of the previously irradiated fuel rods shown in Figures 19 through 21. High fuel temperatures produced considerable fission gas induced porosity with little confirmable fuel melting as shown in Figure 19 (thin band of dense fuel between the porous region and surface unrestructured region may be an indication of fuel melting, or melting could have extended into the porous fuel region). Molten fuel relocation at the surface and within the fuel crack network of the fuel is illustrated in Figures 20 and 21, respectively. Molten UO_2 extrusion and mixing of the melt with solid UO_2 where molten fuel had penetrated the major crack system was typical of the fuel melting observations, but no identifiable evidence of a cylinder of molten fuel, as suggested by FRAP-T5 was found.

4.2 Cladding Phenomena Affecting Fuel Rod Behavior and Failure

Examination of fuel rod debris from Test RIA 1-1 revealed extensive cladding deformation, heavy oxidation, and limited cladding melting and

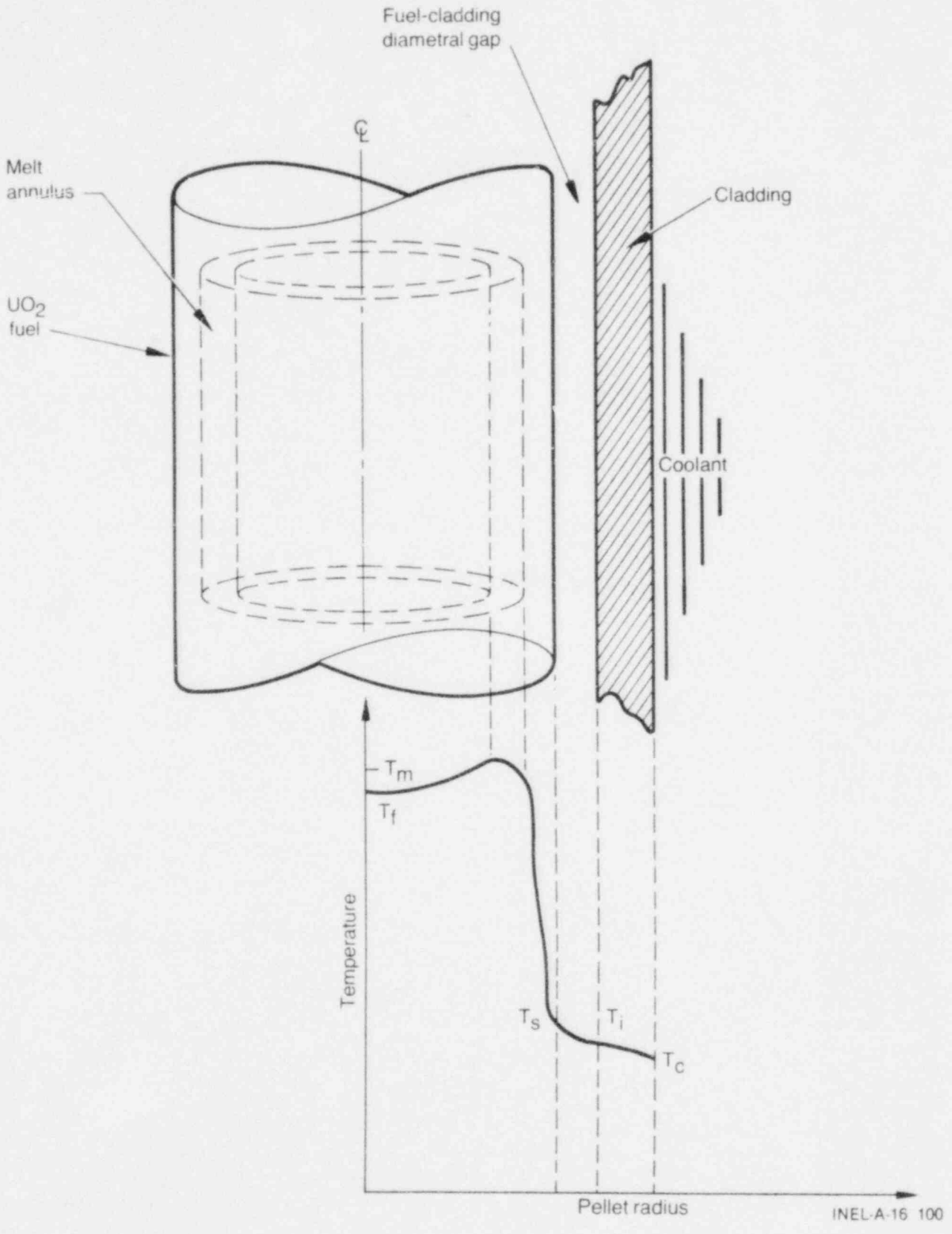

Fig. 18. Conceptual fuel pellet radial temperature profile showing the molten fuel annulus during the RIA transients.

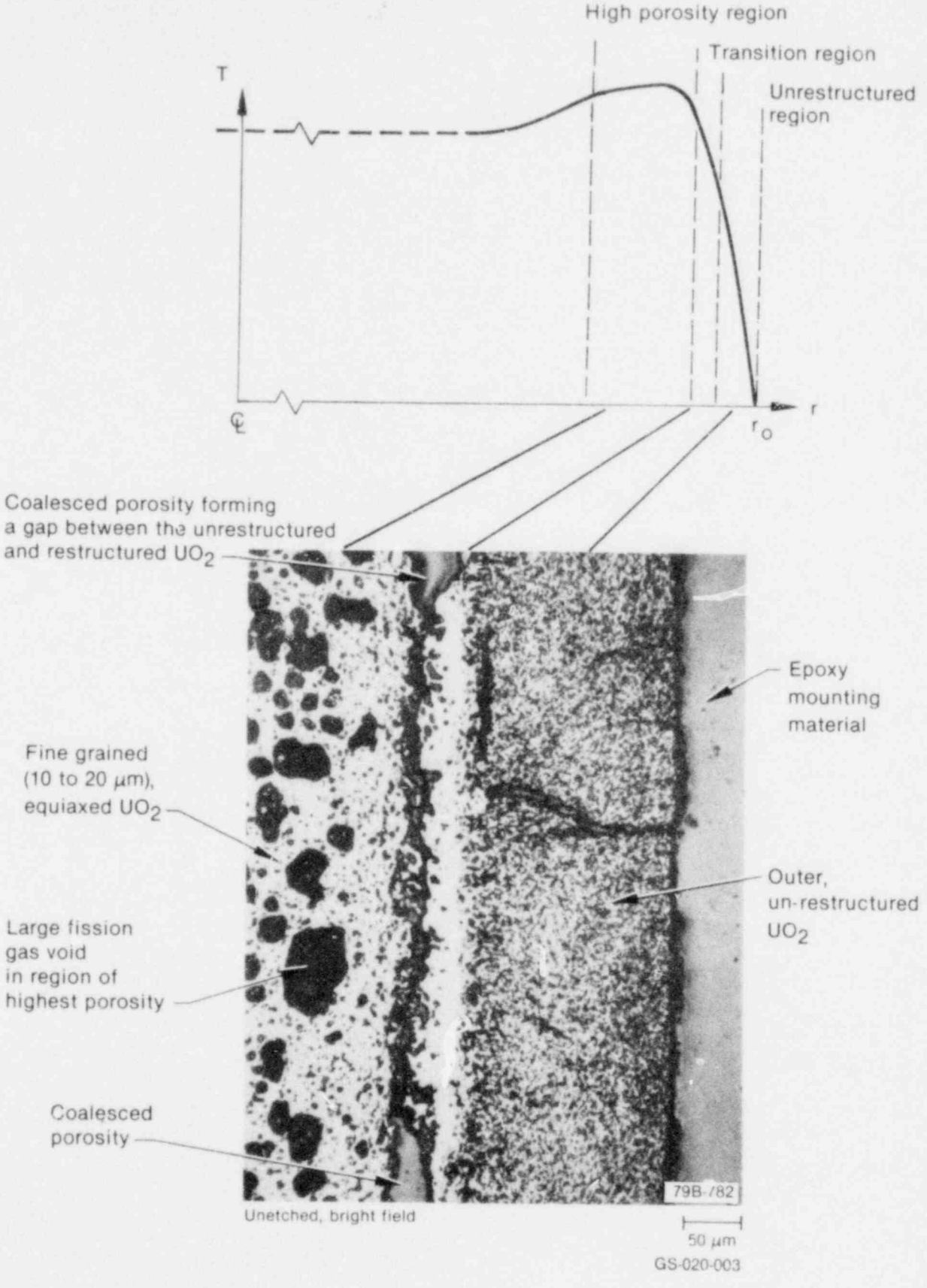

Fig. 19. Irradiated fuel near the pellet surface of previously irradiated Rod 801-1.

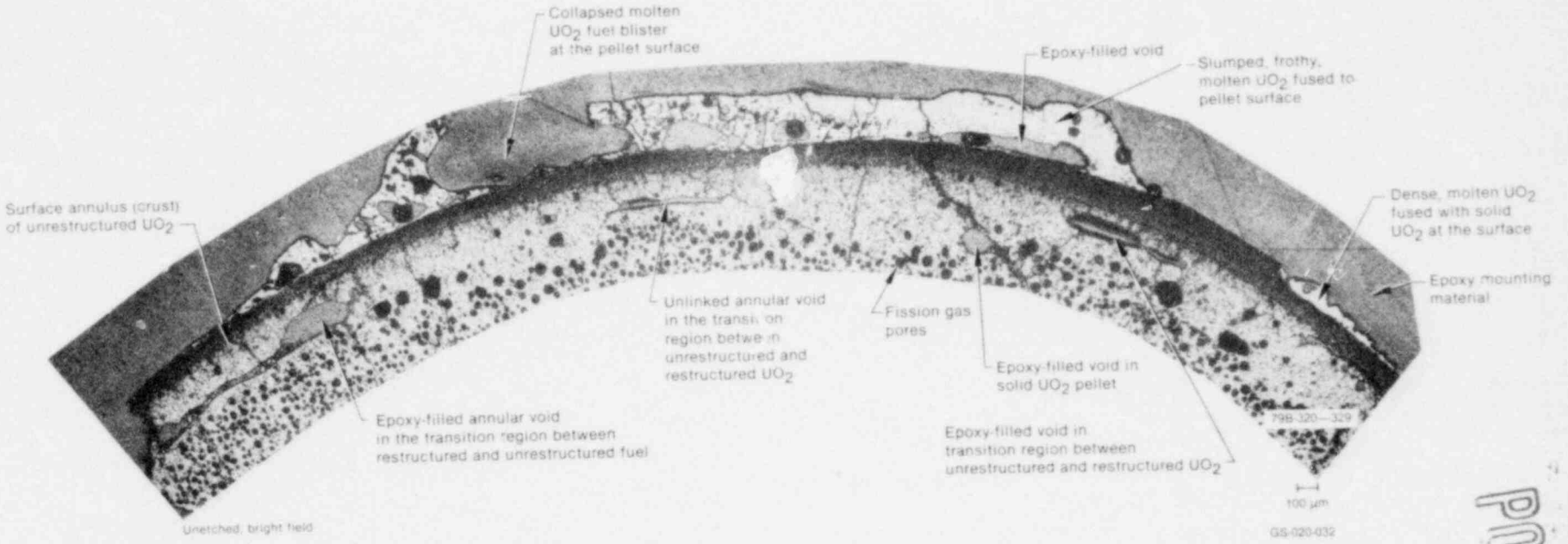

Fig. 20. Pellet fragment from Rod 801-1 showing molten UO_2 frozen to the surface.

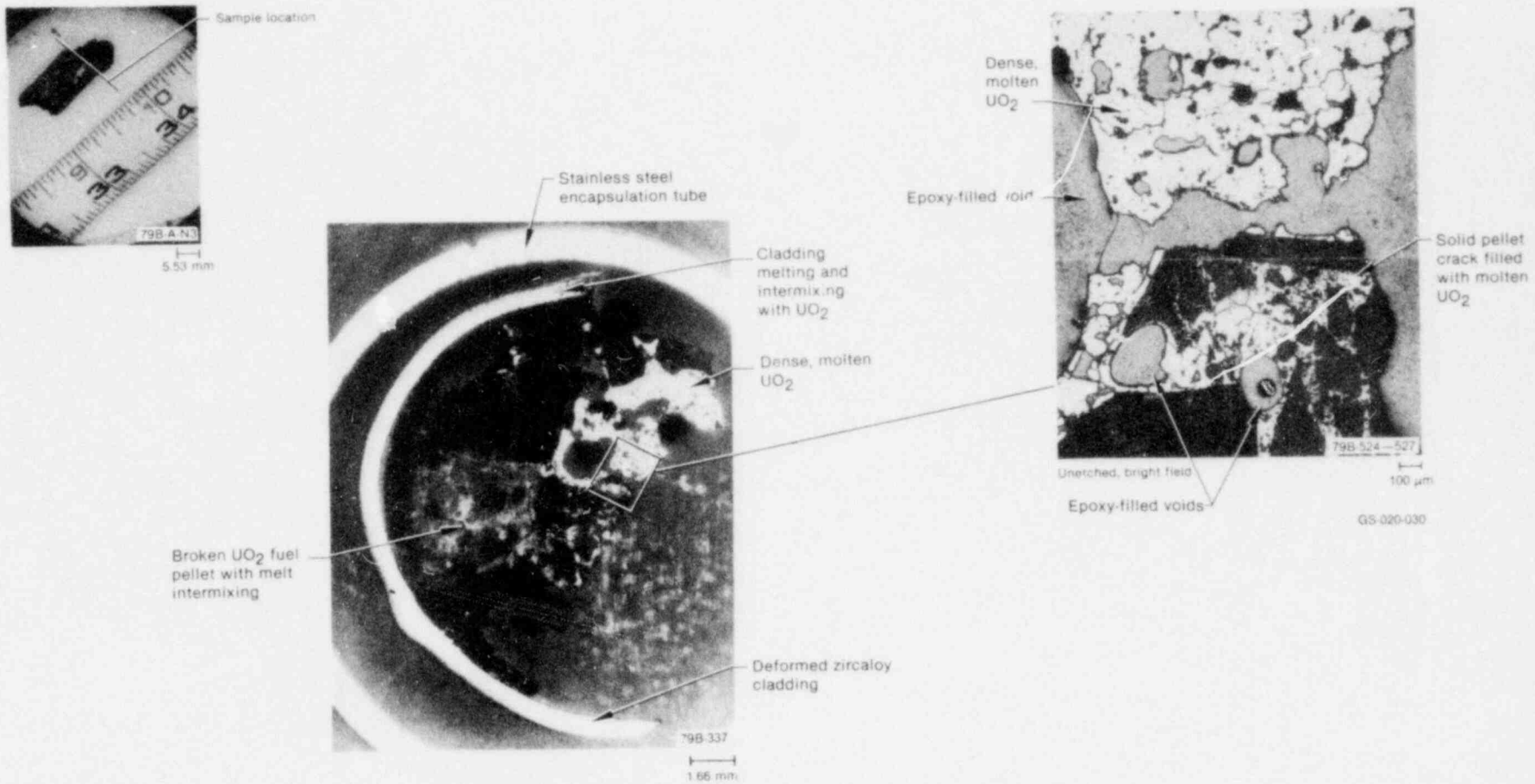

Fig. 21. Molten UO_2 intermixing and fuel crack filling in a rod fragment from Rod 801-2.

intermixing with fuel over the high power region of the test rods. Cladding deformation included rupture and wall thickness variations. The thermal and mechanical response of the test rods to the transient power burst are presented and discussed in this section. The instrumentation responses are compared with FRAP-T5 calculated fuel rod behavior to help assess the validity of the data and also the capability of the code to predict fuel behavior during RIA transients.

High fuel and cladding temperatures during the thermal transient associated with the power burst produced an extended period of film boiling on the cladding surface. Analysis of the on-line data showed that film boiling was detectable by cladding surface temperature and fuel rod axial displacement measurements.[a] Failure of the two previously irradiated test rods was indicated by inlet coolant flow stoppages (zero turbine flowmeter response); failure of one of the previously unirradiated rods was indicated by the plenum pressure transducer. There was no direct indication of failure for the other unirradiated (uninstrumented) test rod, since the displacement transformer on this rod failed prior to the test power burst. Many of the instrument responses illustrated in this section are accompanied by additional dashed-line curves indicating the corresponding FRAP-T5 calculated behavior. The FRAP-T5 calculations were based on a total, radially averaged adiabatic energy deposition of 365 cal/g UO_2 and a radial average peak fuel enthalpy of 285 cal/g. Zero time on each data plot corresponds to the time of peak power during the approximately 50-ms power burst.

4.2.1 Film Boiling

The initiation and propagation of film boiling was similar for the two test rods instrumented with Type S, platinum-rhodium cladding surface thermocouples.[20] The measured temperatures for Rod 801-3 at 0.79 m from the bottom of the fuel stack are shown in Figure 22, together with the FRAP-T5 calculated history. A maximum cladding temperature of 1410 K was measured 1.25 s after the time of peak power. The best estimate cladding

---

a. Fuel rod axial displacements were measured using linear variable differential transformer.

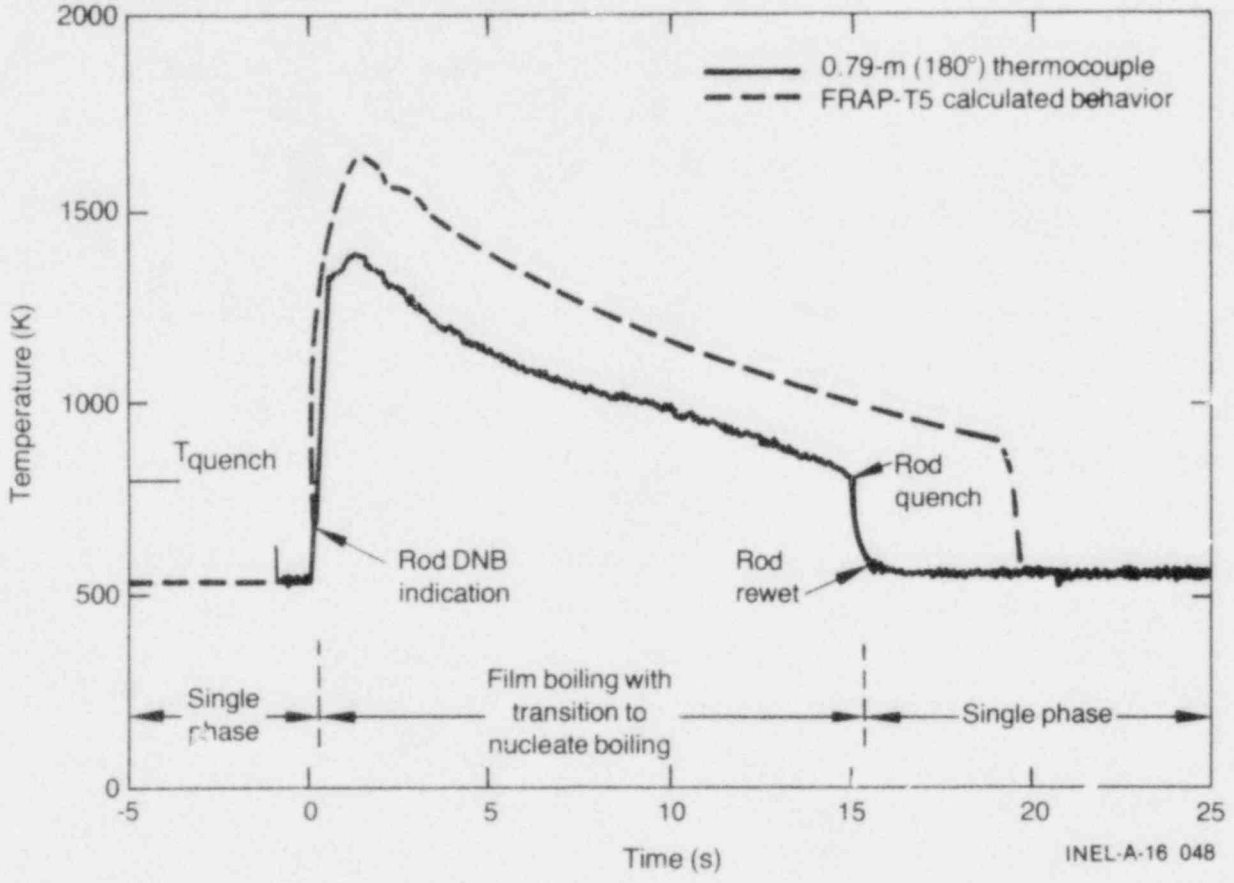

Fig. 22. The 0.79-m, 180-degree cladding surface thermocouple response and the calculated cladding temperature on Rod 801-3.

temperature, calculated using measured oxidation reaction layer thicknesses, was 1380 (± 50) K which is in good agreement with the maximum cladding temperature indicated by the thermocouple. Quenching began about 14 s later, when the thermocouple indicated about 800 K, and continued through to rod rewet at a temperature below about 600 K, within the range of rewet temperatures calculated for the test conditions.[a] The calculated temperature history indicated a maximum cladding temperature of 1662 K at 0.79 m, occurring 1.5 s after the time of peak power. Thus, there is a discrepancy of about 252 K between the measured and calculated surface temperatures, which suggests that a thermocouple cooling fin effect, not modeled in FRAP-T, may have been significant.

---

a. The range of temperatures under which rewet will occur was estimated from the relationship of the interface temperature, T_I, and the wall temperature, T_w, just before rewet, given by[24,25]

$$T_I = \frac{T_W + \sigma T_\ell}{1 + \sigma}$$

where the subscripts I, w, and ℓ refer to the contact interface temperature, the precontact hot wall temperature, and the liquid coolant temperature, respectively; with σ being the coolant-wall thermal ratio, equal to $(k_\ell \rho_\ell C_{p\ell}/k_w \rho_w C_{pw})^{1/2}$, for the liquid coolant, ℓ, and the cladding wall properties. The rewet temperature range was estimated by letting $T_I \sim T_{crit} = 647$ K, the critical temperature of the coolant, and solving for T_w where

$$T_{sat} < T_w \leq T_{crit}\,(1 + \sigma) - \sigma\, T_\ell .$$

For saturated water (and the Test RIA 1-1 conditions) $T_\ell = T_{sat} = 554$ K, and ZrO_2 at the cladding surface, the calculated cladding rewet temperature ($T_w = T_{rw}$) range is about $554 < T_{rw} \leq 700$ K, which is the range indicated by the cladding thermocouple.

4.2.2. Cladding Thermal Expansion

During the period of fuel and cladding high temperatures accompanying the high energy deposition produced by the RIA 1-1 burst, the fuel rods elongated as the temperature increased, and then contracted as the fuel rods cooled. The measured cladding elongation history is illustrated by previously irradiated Rod 801-1 in Figure 23 which failed early during the test. The maximum cladding elongation of Rod 801-1 was 7.3 mm, occurring about 1.25 s after the time of peak power. Based on the flowmeter indication of coolant channel blockage, it was estimated that the fuel rod failed at about 1 to 4 s into the transient, near the time of maximum fuel rod elongation. The times of the maximum displacements were consistent with the measured times of the maximum cladding temperatures. Since the displacement devices respond to thermal excursions at any position on the test rods, the onset of film boiling is reflected in the elongation. Comparison of the elongation and surface temperature histories led to the conclusion that film boiling on Rod 801-1 occurred, at a minimum, over the region spanned by the surface thermocouples, and at approximately the same time.

The FRAP-T5 calculated cladding displacement is plotted as a dashed line in Figure 23 for comparison with the measured elongation response. The calculated cladding elongation follows the change in fuel surface temperatures, exhibiting a decrease in displacement early in the transient (cladding temperature ~600 K). This decrease in elongation is due to an assumption in the FRAP-T5 model of no fuel stack-cladding slippage after gap closure, thus, FRAP-T5 calculates parallel elongation of the fuel and cladding. As a result, as the fuel surface cools briefly due to improved heat transfer after initial contact with the cladding wall, the contracting fuel column forces the cladding into an unrealistic contraction. In contrast, the measured cladding displacement did not exhibit a brief contraction early in the transient. Both the measured and calculated cladding displacements remained positive, and did not return to the original value. The reason the elongation did not return to the original, pre-film-boiling position is attributed to cladding plastic deformation and rod failure, producing residual posttransient displacements.

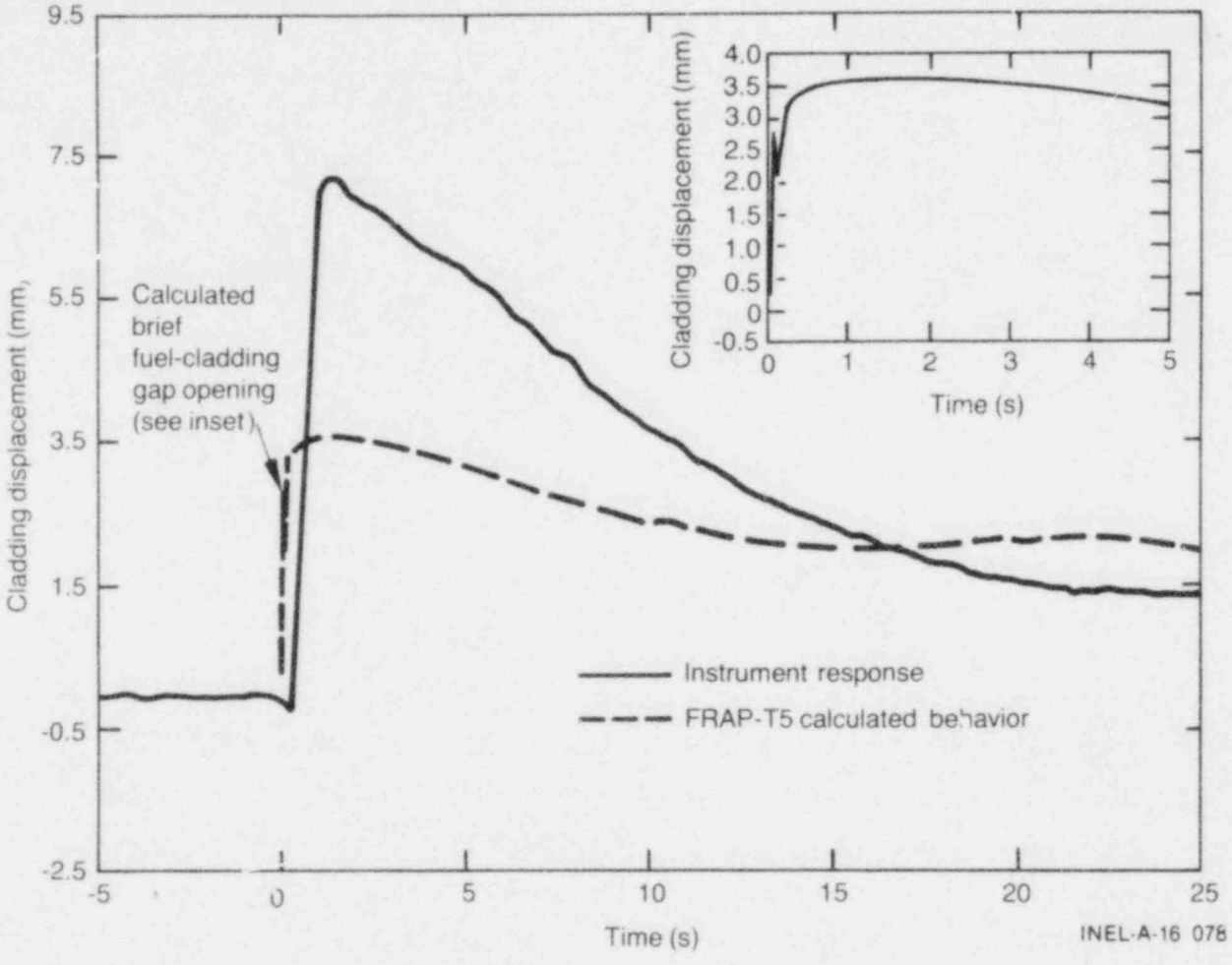

Fig. 23. Cladding thermal displacement of Rod 801-1 during Test RIA 1-1.

4.2.3 Thermal-Mechanical Interaction with the Fuel

In this section the relationship between fuel rod damage and rod thermal condition is examined, and failure modes are described. Fuel stack thermal expansion, leading to high strain rate cladding rupture, was the primary mode of test rod failure. Calculation of the thermal mechanical interaction for Test RIA 1-1 serves as an illustration of the FRAP-T5 analysis.

The rod damage observed during the posttest examination of Test RIA 1-1 included extensive cladding deformation; fuel and cladding melting; irradiated fuel swelling; and zircaloy cladding wall thickness variations, oxidation and embrittlement, and fragmentation. Rapid thermal expansion and fuel swelling fractured and ruptured the cladding during Test RIA 1-1. The contribution of fission gas induced swelling in the previously irradiated rods produced outward distension and bulging of the cladding as demonstrated in Figures 24 and 25.[21]

Cladding diametral deformation produced by hot fuel expansion was significantly different and more extensive in the previously irradiated Test RIA 1-1 fuel rods compared with the unirradiated rods. Deformation was induced by various combinations of thermal expansion, fuel cracking and fragment relocation, fuel melting, and fuel swelling in the previously irradiated rods. Fuel thermal expansion provided a source of axial and radial cladding stress. Fuel melting produced a net volume increase of 4%, and, in previously irradiated rods, fuel swelling resulted from the formation of fission gas bubbles.

The energy deposition accompanying the test power burst and the fuel rod thermal response to the RIA were radially and axially dependent, and the pellet-cladding mechanical interaction (PCMI), established by contact between the thermally distorted fuel and cladding, increased with fuel enthalpy. Multiaxial stresses and high strain rates were produced in the cladding by the thermally expanding fuel, and the cladding failed in

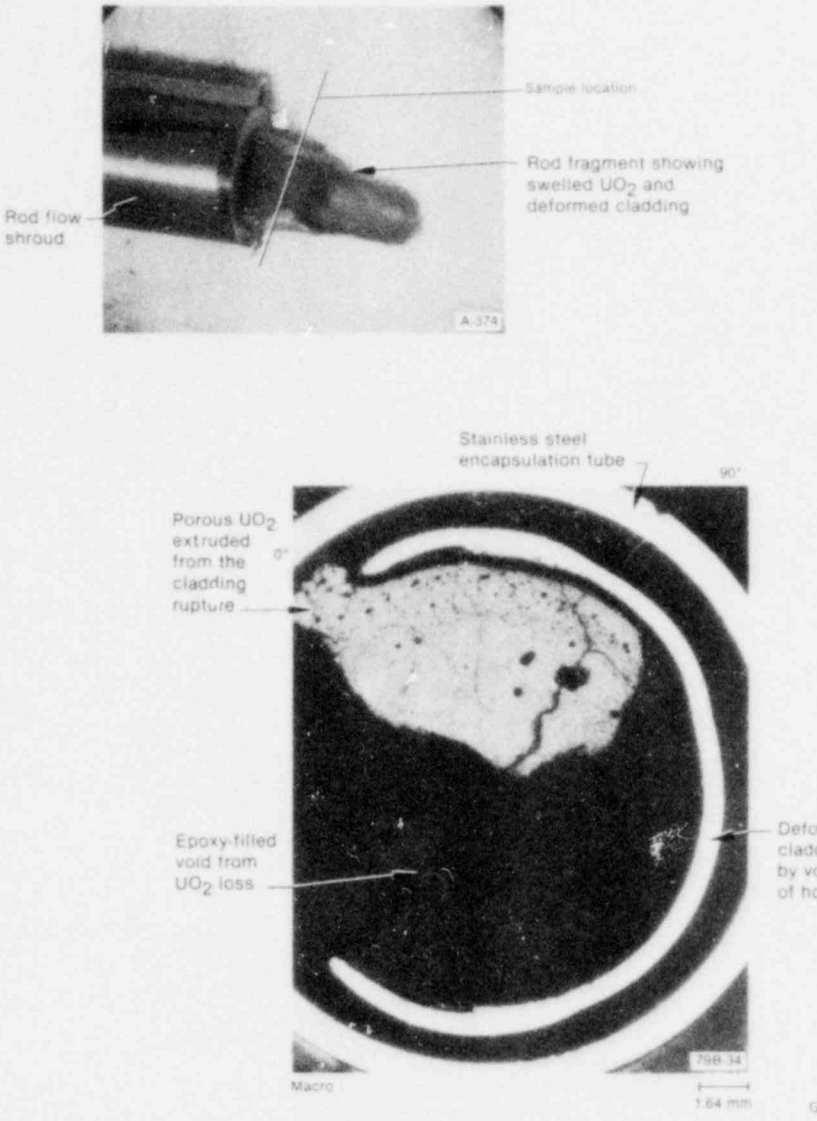

Fig. 24. Cross section of rod fragment exhibiting deformed cladding produced by fuel swelling and extrusion in Rod 801-1.

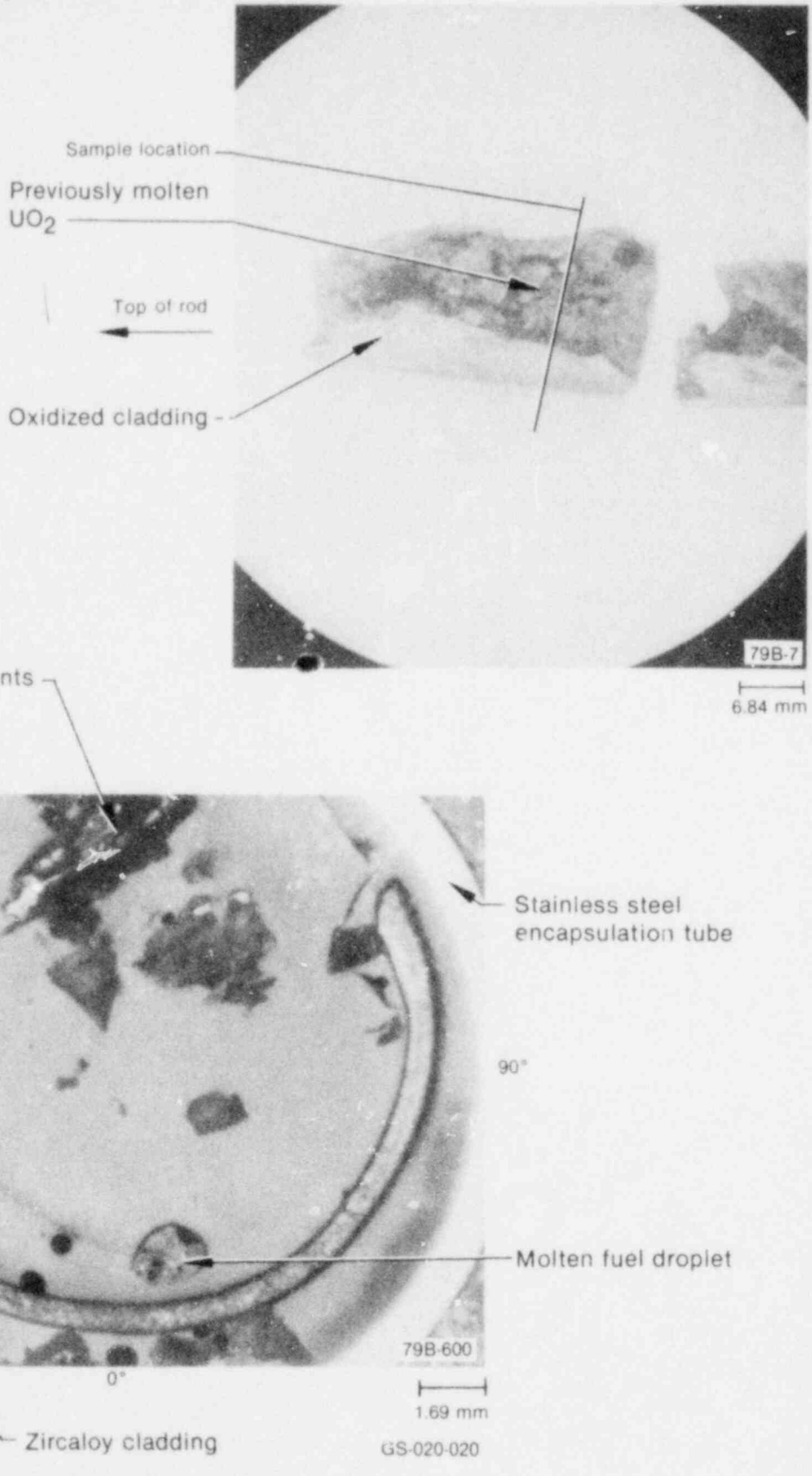

Fig. 25. Rod segment from the region of shroud flow blockage exhibiting rod swelling and fuel-cladding melting.

regions where local stresses exceeded the ultimate strength. The total cladding strain in response to fuel thermal expansion included the elastic, plastic, and free thermal expansion partial strains. Fuel swelling, melting, and densification were generalized to the multiaxial stress state in the calculation by assuming they can be represented as uniform thermal expansion.

To assess the deformation and failure behavior in the test rods, the thermal-mechanical behavior of the rods was determined from computer code calculations using test conditions as input. A detailed thermal-mechanical history of previously irradiated Rod 801-1 was obtained from FRAP-T5 computer calculations and was assumed typical of the behavior of the companion rods in Test RIA 1-1.

The calculated thermal-mechanical history gave an approximate description of the relationship between fuel expansion and increasing cladding strain, stress, and rupture. The fuel-cladding gap width change, cladding hoop stress, cladding hoop strain, and test rod power are plotted in Figure 26 as functions of time for the peak power position. The time of fuel-cladding gap closure, in the calculation, coincided with the time of peak power. The effective cladding hoop stress exceeded the zircaloy yield stress about 3 ms after gap closure, and the cladding was expected to have deformed plastically thereafter. The energy deposition produced a cylinder of molten UO_2 that increased the fuel expansion and the hoop strain. Both the hoop stress and strain follow the variations in fuel thermal expansion associated with expansion of the cylinder of molten fuel and cooling at the pellet surface. The variations arise from the method used in the FRAP-T5 code to couple the fuel and cladding axial and radial expansion behavior.

Failure was predicted by overstress in the cladding at ~17 ms after the time of peak power (prior to the time of reactor scram, the time of peak fuel enthalpy, and the time of significant oxidation). Additional cladding strain produced by thermal expansion of the fuel was assumed to have been accommodated by crack growth in the ruptured cladding. Gap

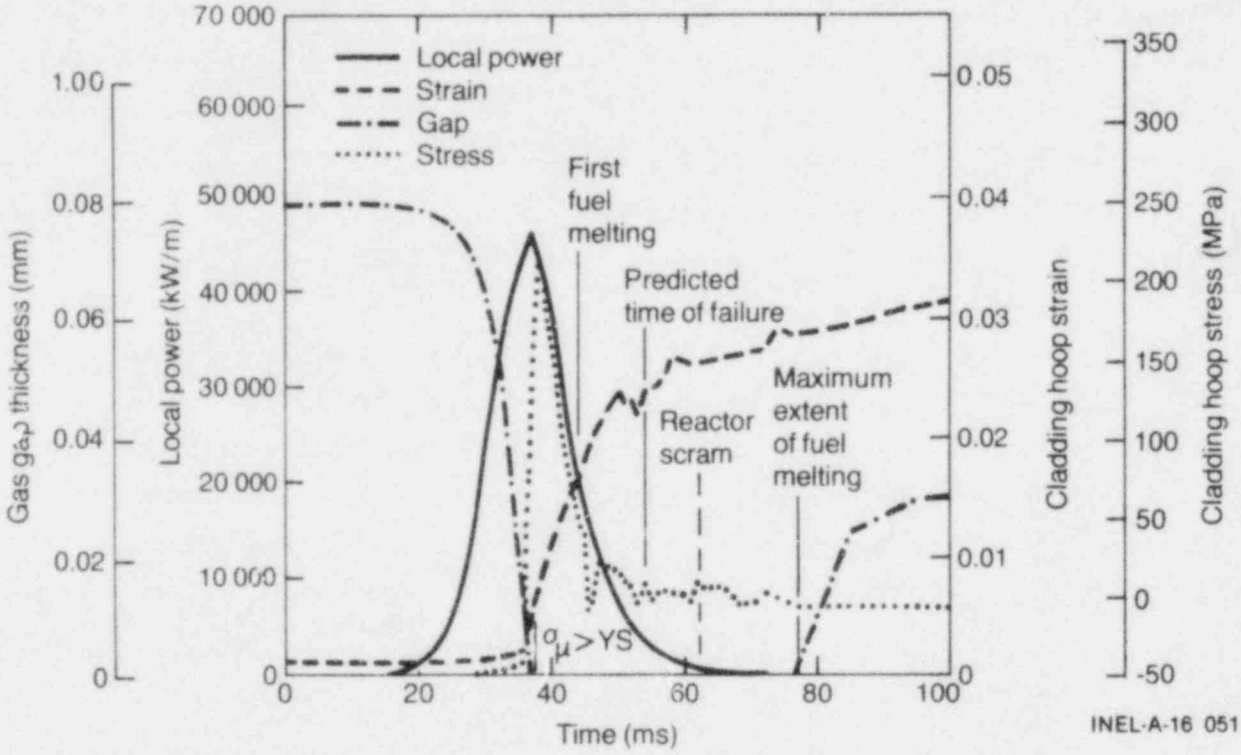

Fig. 26. Fuel rod power and FRAP-T5 calculated change in fuel-cladding gap at the axial peak flux position, with associated changes in the cladding hoop stress and strain through rod failure for Rod 801-1.

closure, at the time of predicted failure, was calculated to extend along the rod from about 0.17 to 0.53 m from the bottom of the fuel stack, and to comprise about 30% of the fuel stack length.

The predicted cladding hoop stress, and strain behavior, are plotted in Figure 27 with the fuel and cladding surface temperatures. Failure by overstress was calculated to occur for cladding surface temperatures near 885 K. The cladding inner surface temperature (not shown in the figure) was near 1400 K, due to fuel-cladding contact. The average wall temperature of 1140 K (α + β two-phase zircaloy temperature region) is above the temperature region in which a superplasticity maximum in the zircaloy exists at ~1093 K, and in which large hoop strains, uniform wall thinning, and axial contractions are expected to occur.[26] The calculated radially averaged fuel enthalpy at the time of predicted cladding failure was nominally 281 cal/g (peak local fuel enthalpy of 317 cal/g).

The multiaxial stress state in the cladding up to and after failure is suitably approximated by the biaxiality (defined as the ratio of the tangential or hoop stress to the axial stress). The FRAP-T5 calculations of the rod mechanical history showed that a biaxiality ratio of ~2.0 is maintained until fuel-cladding gap closure, as shown in Figure 28. The large changes in cladding biaxiality indicate that the cladding stresses are complexly related to the combined effects of PCMI and coolant pressure. The FRAP-T5 calculation provides a remarkably accurate description of the mechanical failure of the rods by overstress, considering that the mechanical models were based on slower strain rate materials data ($\sim 10^{-3}$ - 10^{-4} s^{-1}), primarily intended for the loss of coolant accident time frame.

The deformation processes interpreted from Figures 26, 27 and 28 involve high strain rates ranging from 0.15 s^{-1} before gap closure, to 2.1 s^{-1} when the yield stress is exceeded (3 ms after gap closure), followed by a decrease to 0.64 s^{-1} as the cladding begins to deform plastically (temperature dependence of the yield strength).[5] Fuel melting produces a second, rapid increase in the strain rate (up to about

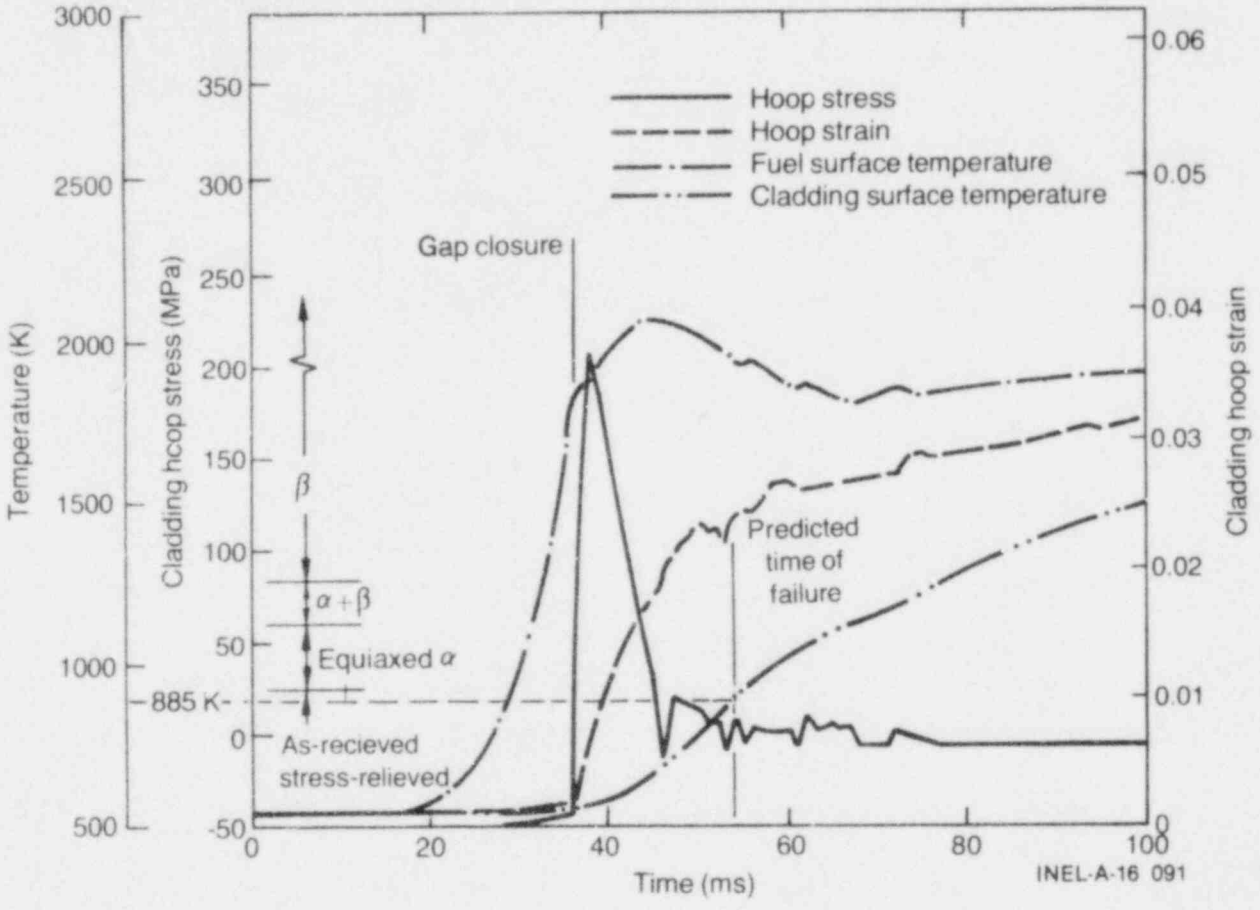

Fig. 27. Calculated fuel rod stress-strain behavior showing failure when the cladding surface temperature is below the recrystallization temperature (920 K) of the equiaxed α phase.

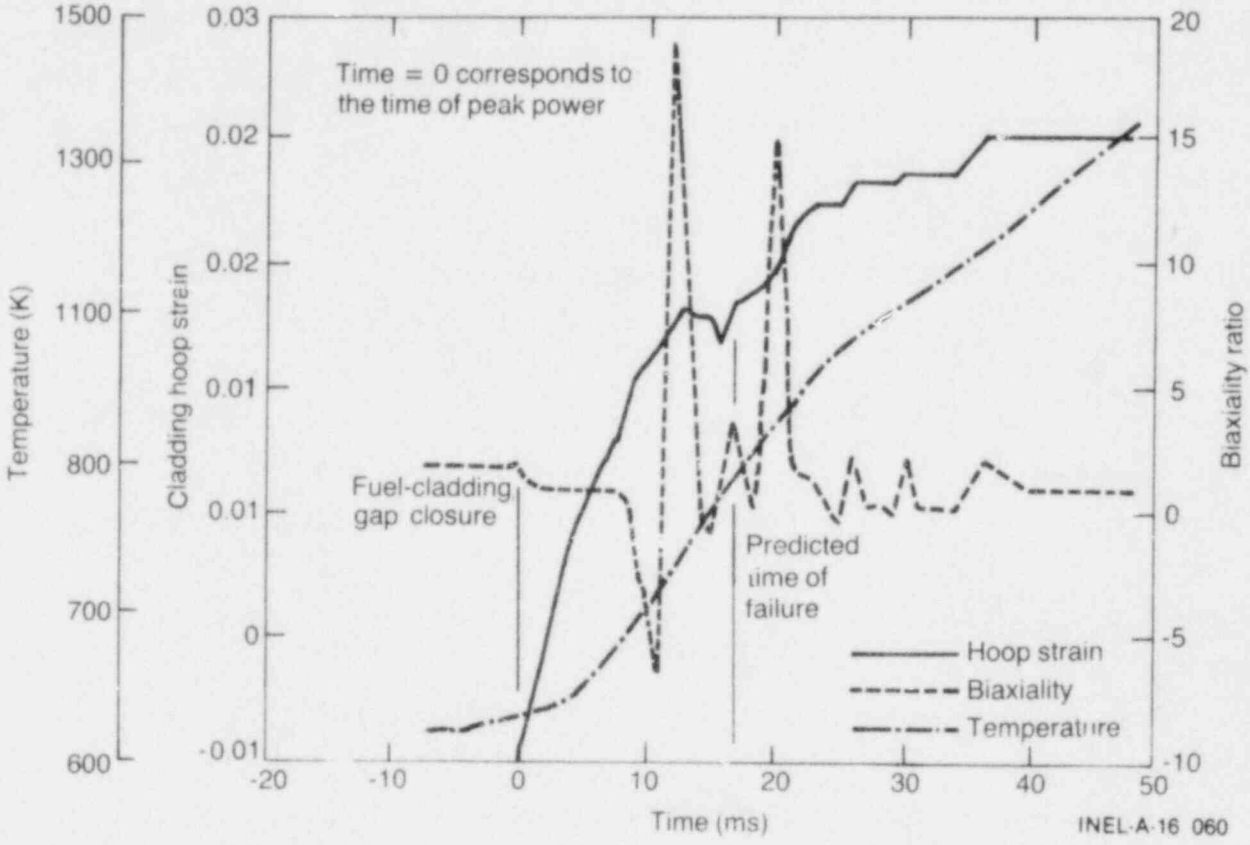

Fig. 28. The effect of biaxiality and temperature on cladding hoop strain during the time to rupture.

3.1 s^{-1}), which is followed by a rapid change in the biaxiality. Such rapid changes in strain rate might be expected to produce strain rate hardening (an inelastic response) as the fuel heating and radial expansion continue, up to failure (at a strain rate of 2.2 s^{-1}). Evidence of the high strain rate behavior of the cladding was found in the postirradiation examination.

The wall fracturing typically observed in the Test RIA 1-1 cladding supports the view that low cladding temperatures and texture play a role in the high strain-rate rupture. Due to the very high strain rate deformation imposed by the RIA 1-1 transient, too little time was available to accommodate cladding straining, and higher cladding temperatures than noted are required to achieve similar levels of effective strain without failure. The through-wall failures shown in Figures 29 and 30 for previously irradiated Rod 801-2 exhibit angular fracture. The FRAP-T5 calculations emphasize that appropriate conditions for overstress failure exist only during the earliest times of the RIA transient. The presence of oxide on the fracture surfaces of the cladding in Figures 29 and 30 supports the view of early failure prior to the onset of film boiling conditions, and thus support the calculated behavior.

4.3 Conclusions Concerning the Calculated Fuel and Cladding Behavior

A comparison of the calculated and measured fuel rod behavior for an RIA shows that:

(1) The FRAP-T calculated temperature histories of the fuel emphasize that energy deposition near the outer surface of the fuel pellet has a dominant effect on the heat flux out of the fuel during the early portion of the transient, and thus strongly influences the maximum cladding temperature. This result is supported by the posttest metallographic observations of fuel damage.

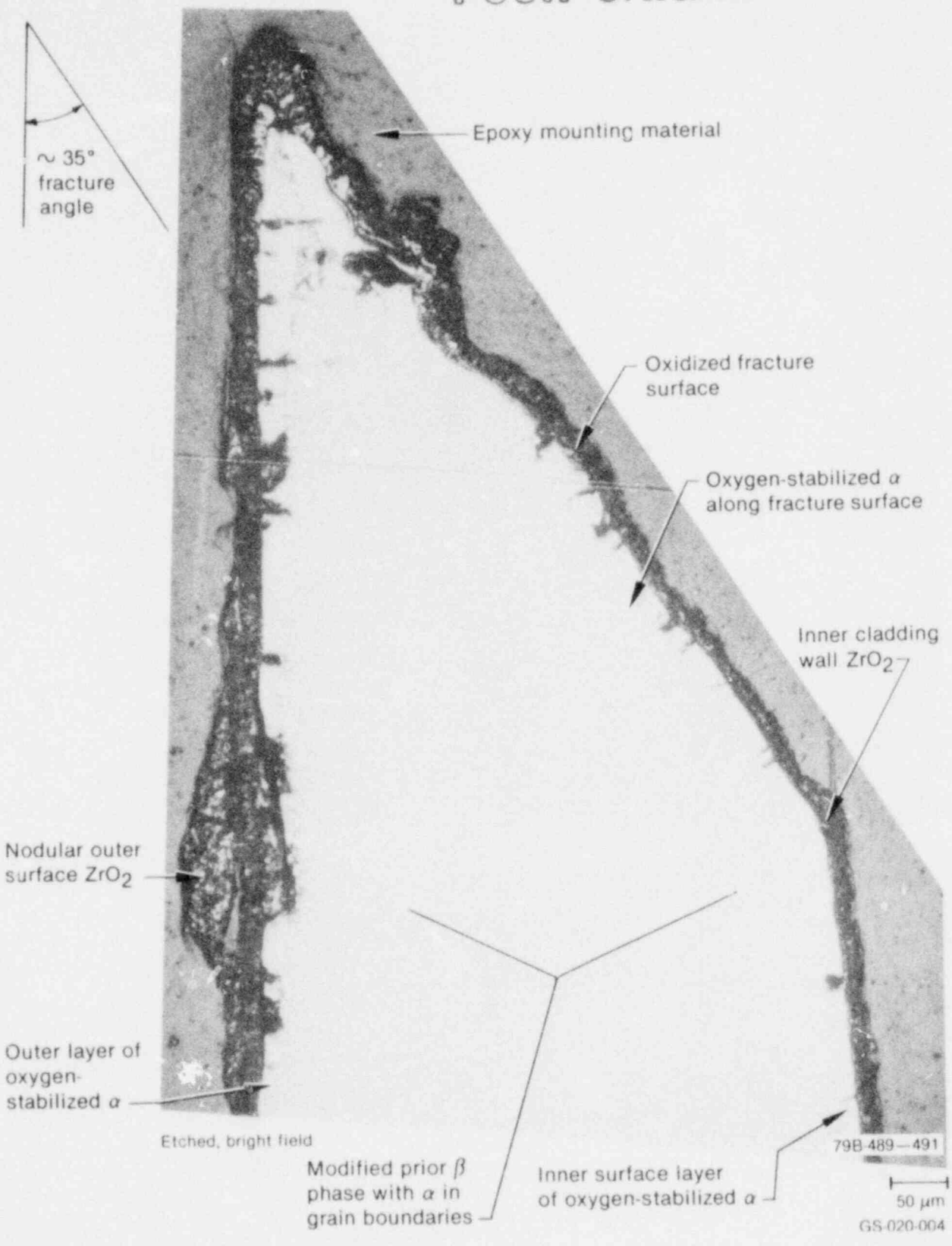

Fig. 29. Through-wall fracture of Rod 801-2 exhibiting surface oxidation.

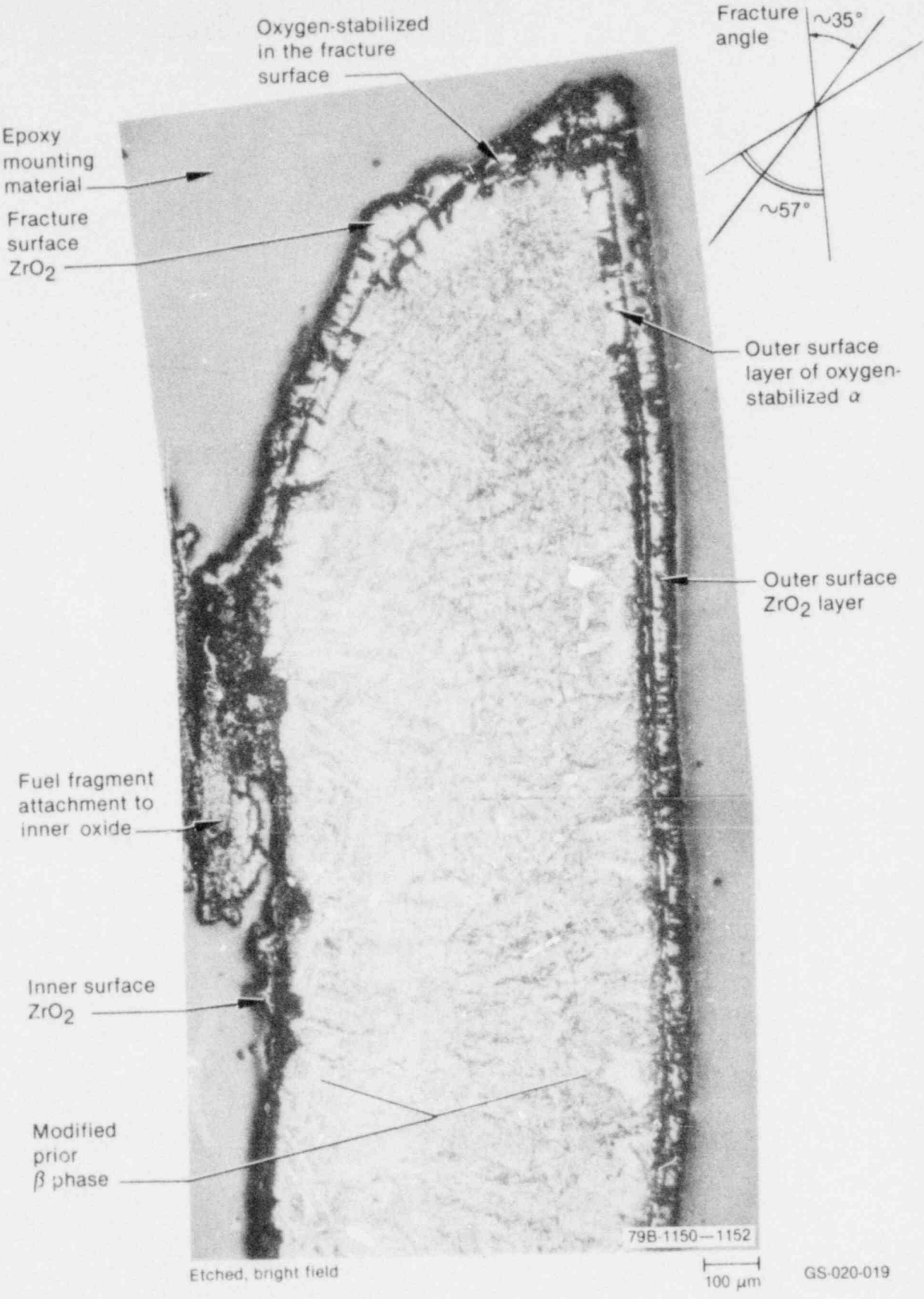

Fig. 30. Oxidized fracture surface in Rod 801-2.

(2) The FRAP-T calculated fuel centerline temperature is in reasonable agreement with the measured fuel centerline temperature, when compensation for thermocouple response time is taken into account.

(3) FRAP-T5 overcalculates the amount of molten UO_2 present at the axial power peak location in a test fuel rod subjected to an enthalpy insertion of 285 cal/g during an RIA at BWR hot startup conditions.

(4) The measured temperatures were lower than the calculated peak cladding surface temperatures, suggesting that other effects, such as thermocouple cooling fin effects, were significant. FRAP-T5 does not contain a thermocouple compensation model. Thermocouple data should be adequately compensated for error prior to comparison with FRAP-T calculated temperatures.

(5) The calculated thermal-mechanical history determined by FRAP-T5 provided an approximate description of the relationship between fuel expansion and increasing cladding strain, stress, and rupture. Some variations in the behavior calculated by FRAP-T arose from the method used by the code to couple fuel and cladding axial and radial expansion, suggesting that the code may have modeling deficiencies such as in describing fuel stack-cladding slippage after gap closure and high strain-rate materials properties in calculating the fuel behavior for very rapid changes in conditions as induced by an RIA.

5. CONCLUSIONS

An understanding of fuel response to normal operation and off-normal hypothesized reactor transients in light water reactors is an important consideration in reactor safety studies. This report has presented the analyses, interpretation, and discussion of results of steady state gap conductance tests performed to measure the effects of fuel rod internal pressure and fill gas composition on fuel temperature, and the results of transient RIA tests performed to determine the extent of fuel rod damage and modes of fuel rod failure. Test fuel rod behavior was assessed from comparisons of FRAP-T5 calculated behavior with instrumentation response data and posttest metallurgical observations. In this section, conclusions concerning the comparisons made between FRAP-T calculations and measured fuel rod behavior are presented.

The major conclusions obtained from this study are summarized for the steady state gap conductance tests as follows:

1. FRAP-T5 generally over predicted fuel centerline temperatures by 3 to 7%, within the experimental error, for a range of xenon concentrations (0 to 10%) in helium fill gas. Divergence of the calculated centerline temperatures from measured values at high xenon concentrations may be attributed to model limitations in the option chosen for comparison. Other models currently in FRAP-T need to be investigated for a better assessment of the FRAP-T performance.

2. For the measured effects of fuel rod fill gas pressure and composition on the steady state fuel temperatures, FRAP-T calculations showed good agreement with data for fill gas pressures in the range 0.1 to 5.0 MPa with gas compositions ranging from pure helium to helium with 10% xenon, with one exception, where the fuel behavior underwent a change above 2.0 MPa in the wide gapped (0.23 mm) test rod.

Conclusions for the transient fuel rod behavior are summarized as follows:

1. The mode of fuel rod failure for rods tested at 285 cal/g during an RIA event was strongly affected by previous irradiation and the peak fuel enthalpy. Failure and loss of rod geometry occurred in both irradiated and unirradiated rods due to mechanical overstraining of the cladding, followed by partial or total cladding wall melting and oxidation embrittlement. The FRAP-T calculated rod temperature histories of the fuel and the posttest metallographic observations emphasized the effect of energy deposition near the outer pellet surface on the heat flux out of the rod which strongly influenced the maximum temperature of the cladding.

2. Fuel centerline temperatures calculated by FRAP-T were in reasonable agreement with the measured values throughout the RIA transient when the thermocouple response was taken into account. Comparison of measured cladding surface temperatures with the FRAP-T5 calculated temperatures showed that the calculated temperatures were higher than measured values, suggesting that other effects, such as thermocouple fin effects, were significant. The FRAP-T code currently does not model such thermocouple effects.

3. FRAP-T5 overpredicts the amount of radial and axial fuel melting in UO_2 (nominally 94% theoretical density) subjected to an enthalpy insertion of 285 cal/g during an RIA at BWR hot startup conditions.

4. Pellet-cladding mechanical interaction induced failure due to high strain rate deformation was correctly indicated from the thermal-mechanical history calculated by FRAP-T5. Some variations in the calculated deformation and rod elongation behavior arose from the method used by the computer code to

couple fuel and cladding axial and radial expansion, suggesting that the code may have some modeling deficiencies in describing the fuel behavior for very rapid changes in fuel rod behavior induced by an RIA.

6. REFERENCES

1. L. J. Siefken, M. P. Bohn, S. O. Peck, and J. A. Dearien, FRAP-T5: A Computer Code for the Transient Analysis of Oxide Fuel Rods, NUREG/CR-0840, TREE-1281, June 1979.

2. T. E. Murley, L. S. Tong, and G. L. Bennett, Summary of LWR Safety Research in the USA, Report presented at the International Conference on Nuclear Power and its Fuel Cycle, May 2-13, 1977, Salzburg, Austria, NUREG-0234.

3. United States Nuclear Regulatory Commission, Water Reactor Safety Research Program, A Description of Current and Planned Research, NUREG-0006, February 1979.

4. M. K. Charyulu, A Review of FRAP-T4 Performance Based on Fuel Behavior Tests Conducted in the PBF, EGG-TFBP-5010, September 1979.

5. D. L. Hagrman, G. A. Reymann, and R. E. Mason, Eds., MATPRO-Version 11 (Revision 0): A Handbook of Materials Properties for Use in the Analysis of Light Water Reactor Fuel Rod Behavior, NUREG/CR-0497, TREE-1280, Rev 0, February 1979.

6. J. Rest, GRASS-SST: A Comprehensive Mechanistic Model for the Prediction of Fission Gas Behavior in UO_2 Based Fuels During Steady State and Transient Conditions, NUREG/CR-0202, ANL-78-53, June 1978.

7. Aerojet Nuclear Company, RELAP4/MOD5: A Computer Program For Transient Thermal-Hydraulic Analysis of Nuclear Reactors and Related Systems, Vols I-III, ANCR-NUREG-1335, September 1976.

8. G. A. Burna, M. P. Bohn, and D. R. Coleman, FRAPCON-1: A Computer Code for the Steady State Analysis of Oxide Fuel Rods, CDAP-TR-78-032-R1, November 1978.

9. J. A. Dearien et al., FRAP-S3 Analytical Models and Input Manual: FRAP-S3 A Computer Code for the Steady State Analysis of Oxide Fuel Rods, Vol. 1, Rev. 2, TFBP-TR-164, March 1978.

10. C. R. Hahn, C. E. Beyer, and L. J. Parchen, GAPCON-THERMAL-1: A Computer Program for Calculating the Gap Conductance in Oxide Fuel Pins, BNWL-1778, September 1973.

11. C. E. Beyer et al., GAPCON-THERMAL-2: A Computer Program for Calculating the Thermal Behavior on an Oxide Fuel Rod, BNWL-1898, November 1975.

12. R. W. Miller and A. D. Appelhans, Measured Effects of Fuel Rod Internal Gas Pressure and Xenon Concentration in Operating Fuel Rods and a Comparison with Basic Theory and FRAP Calculations, EGG-TFBP-5222, August 1980.

13. B. B. Peeler et al., Independent Assessment of the Transient Fuel Rod Analysis Code FRAP-T5, EGG-CAAP-5074, December 1979.

14. A. M. Ross and R. L. Stoute, Heat Transfer Coefficient Between UO_2 and Zircaloy-2, AECL-1552, June 1962.

15. MATPRO-Version 10, A Handbook of Material Properties for Use in the Analysis of Light Water Reactor Fuel Rod Behavior, TREE-NUREG-1180, 1978.

16. J. M. Gandhi and S. C. Saxena, "Correlated Thermal Conductivity Data of Rare Gases and Their Binary Mixtures at Ordinary Pressures," Journal of Chemical and Engineering Data, 13, 3, 1968.

17. A. D. Appelhans, et al., Cracking and Relocation of UO_2 Fuel During Initial Nuclear Operation, NUREG/CR-0247, TREE-1208, July 1978.

18. D. L. Hagrman, Gas Thermal Conductivity (GASCON, GTHCON, GJUMP), EGG-CDAP-5029, October 1979.

19. United States Nuclear Regulatory Commission, A Description of Current and Planned Reactor Safety Research Sponsored by the Nuclear Regulatory Commission's Division of Reactor Safety Research, NUREG-75/058, June 1975.

20. R. S. Semken, et al., Reactivity Initiated Accident Test Series, RIA Scoping Tests, Fuel Behavior Report, NUREG/CR-1360 EGG-2024, April 1980.

21. S. L. Seiffert, et al., Reactivity Initiated Accident Test Series, Test RIA 1-1, (Radial Average Fuel Enthalpy of 285 cal/g), Fuel Behavior Report, NUREG/CR-1455, EGG-2040, September 1980.

22. G. A. Tator, Thermocouple Response Analysis for PBF RIA 1-4 and PR-1 Test Transients, RE-A-80-073, July 1980.

23. D. R. Olander, Fundamental Aspects of Nuclear Reactor Fuel Elements, TID-26711-P1, April 1979.

24. P. J. Berenson, "Transition Boiling Heat Transfer from a Horizontal Surface," MIT Technical Report No. 17, March 1960.

25. F. S. Gunnerson and D. T. Sparks, Behavior of a Nine-Rod Fuel Assembly During Power-Cooling Mismatch Conditions, Results of Test PCM-5, NUREG/CR-1103, EGG-2002, November 1979.

26. H. M. Chung and T. F. Kassner, Deformation Characteristics of Zircaloy Cladding in Vacuum and Steam Under Transient Heating Conditions: Summary Report, NUREG/CR-0344, ANL-77-31, July 1978.

APPENDIX

FRAP-T COMPUTER CODE INPUT

APPENDIX

FRAP-T COMPUTER CODE INPUT

The FRAP-T5 computer code is a modular code composed of a number of subcodes that may be used to iteratively calculate the integral fuel rod behavior. The program was used to determine fuel radial temperature profiles, fuel rod axial temperature profiles, fuel cladding gap conductance, fuel and cladding deformation, and rod internal pressures to assess the capability of the code to predict measured fuel rod behavior.

This appendix contains the fuel rod input parameters used in the steady state and transient FRAP-T calculations.

POOR ORIGINAL

1. GAP CONDUCTANCE CALCULATIONS

```
         1         2         3         4         5         6         7         8
12345678901234567890123456789012345678901234567890123456789012345678901234567890

  1    1    5    0    0    1    0    1    2    0    0    0    0    0
  1    0    0    0    0    0    0    0
     0.8       64.        1.0       1.     1.2837   .012789       300.       0.1
 10421.5  0.005341        0.0  12.7E-3       0.0        C.0       C.0
  2.
 1.026     1.2837
                                  1.E-6
  1             1  1.0
  0     0       0
 100   100    50   50     1
     290.      3000.      290.      2500.
* IFA-430 ROD 2,  230 MICRON DIAMETRAL GAP.
* GENERAL DATA FOR HEAT-1
01010001     10    2    0.0    1.0    200    1.0    200
* GEOMETRY LOCATION AND MESH INCREMENT
01010200        0
* MESH INCREMENT DATA - UNITS ARE METERS
01010201     1  0.00094     5  0.0053404     1    0.00545    2    0.000395
* COMPOSITION OVERLAY
01010301        L      6      3      7      2      9
* SOURCE POWER RADIAL DISTRIBUTION CARDS
     01010401      0.892  1    0.905   2    0.933   3    0.972   4   1.038   5
01010402      1.106   6    0.0   7    0.0   8    0.0   9
* INITIAL TEMPERATURE DISTRIBUTION
01010601      390.    10

  1    2    6
    .001          0.         40.0        100.
    0.93          0.         0.98         .26      1.15      .53      1.26      .79
    1.04        1.05         0.74        1.32
  0    2           2          2
  3.45E6         0.0       3.45E6       1000.
  1.999E6        0.0       1.996E6      1000.
  2.00E6         0.0         2.E6       1000.
    700.         0.0         700.       1000.
  0.0748
  .02549
 .008756
  1.1      2.2          10.0     .06E7        0.1     7.9E-3      1.E-3      257.
  1     30                    0.05
  0.95
   5

        *** OD CODE GENERAL INPUT ***

INPUT IS IN S. I. UNITS
NUMBER OF FUEL RODS            =
NUMBER OF FLOW CHANNELS        =   1
NUMBER OF AXIAL NODES          =

FUEL DEFORMATION MODEL TYPE    =    2
FREE THERMAL EXPANSION FUEL DEFORMATION MODEL SPECIFIED

METAL-WATER REACTION CALCULATIONS SUPPRESSED

MODIFIED ROSS AND STOUTE MODEL FOR GAP CONDUCTANCE TO BE USED

GAS FLOW MODEL NOT TO BE USED - INSTANT PRESSURE EQUILIBRIUM ASSUMED
```

*** NO DIALS TURNED ON ***

****

********** REFLOOD FLAG IS SET TO OFF

****

SUMMARY OF THE LACE SPECIFICATIONS WITH THE SPECIFIED OPTION NONE

1	OFF
2	OFF
3	OFF
4	OFF
5	OFF
6	OFF
7	OFF
8	OFF
9	OFF
10	OFF
11	OFF
12	OFF
13	OFF
14	OFF
15	OFF
16	OFF
17	OFF
18	OFF
19	OFF
20	OFF
21	OFF

****

GENERAL DATA

HEAT PROBLEM NUMBER = 1

NUMBER OF MESH POINTS = 10

GEOMETRY TYPE = CYLINDRICAL

LEFT BOUNDARY COORD. = 0.

SOURCE SCALING FACTOR = 1.000000E+00

TOTAL INTEG. SOURCE = 9.79157E-04

DATA FOR STEADY STATE CALCULATIONS

MAX NO. OF ITERATIONS = 200

CONVERGENCE CRITERION = 1.000000E-00

DATA FOR TIME DEPENDENT CALCULATIONS

MAX NO. OF ITERATIONS = 200

CENTRAL VOID PRESCRIBED FOR FUEL

RADIUS OF CENTRAL VOID = .309396E-02 FT .960002E-03 M

LOWER ELEVATION OF CENTRAL VOID = .330619E+04 FT .102600E+01 M

UPPER ELEVATION OF CENTRAL VOID = .421161E+01 FT .125370E+01 M

*** COOLANT CONDITIONS ***

NSWC = 0 ENTHALPY RISE OF COOLANT WHILE FLOWING PAST FUEL RODS TO BE COMPUTED BY FRAP-T

CRITICAL HEAT FLUX OPTION = 0 COLD WALL * (SI AXIAL FLUX SHAPE

C - H - F CORRELATION = 0 HUGHES/(BARNETT/GELLERSTADT(B&W))

POST-CHF HEAT TRANSFER CODE = 0 DENSEVELLE EQN, S.V AS MODE 5.

NUMBER OF GRAM-MOLES OF GAS IN FUEL ROD # 1 = .242962E+04

COLD STATE VOID VOLUME OF FUEL ROD ******* INCH**3 .100000E+11 ****3

2. REACTIVITY INITIATED ACCIDENT CALCULATIONS

```
         1         2         3         4         5         6         7         8
12345678901234567890123456789012345678901234567890123456789012345678901234567890
   1    1   -12    0   16    1    1    0    3    0    0    0    0    0
   0    0     0    0    0        14    1    0
0.0          1.0                          0.9105      0.009577    300.
10408.       0.00330     0.000343   0.01517   1.1788E-080.0        397440.
2.0          1883.
1.001        1.001                                                 0.5
0.002        0.0         0.002      0.020     0.001       0.0201      0.001     0.070
0.002        0.0701      0.002      0.100     0.005       0.1001      0.005     0.200
0.010        0.2001      0.010      0.300     0.050       0.3001      0.050     0.500
0.100        0.5001      0.100      10.0      0.200       10.001      0.200     25.0
    1            11.0
1.04         1.12        0.20       0.275     0.34        0.4318      0.46      0.53
0.619        0.71        0.79       0.867
    0     0      0
0.002        0.0         0.002      0.020     0.001       0.021       0.001     0.070
0.010        0.080       0.010      0.200     0.050       0.250       0.050     0.500
0.100        4.000       0.100      1.500     0.500       2.000       0.500     5.000
1.00         6.00        1.00       25.0
  100   100    50    50
290.         3290.       290.       2290.
*  MESH SENSITIVITY STUDY  10 FUEL MESH SPACINGS
01010001   14 2 0.0 1.0 200 0.5 200
01010200   0  1
01010201   1 0.00192  1 0.0027149  1 0.0031835  1 0.0035915  1 0.0037175
01010202   1 0.0038394  1 0.0039576  1 0.0040723  1 0.0041842  1 0.004293
01010203   1 0.004375  2 0.004989
01010301   1 10  3 11  2 13
01010401   0.920166 1  0.953252 2  0.982202 3  1.007017 4  1.023560 5
01010402   1.037838 6  1.073253 7  1.110507 8  1.147761 9  1.185014 10
01010403   0.0 11  0.004 13
01010601   538. 14
*
    1    48    18
0.62396      0.0         1.0555     0.0011    2.0860      0.0027      4.0418    0.0048
9.1200       0.00675     22.066     0.00925   52.368      0.01175     183.36    0.01540
424.68       0.0178      976.79     0.0202    2220.9      0.0226      4926.7    0.025
10382.       0.0274      19667.     0.0298    27649.      0.0314      38865.    0.0338
43828.       0.037       38871.     0.0394    29793.      0.0418      20476.    0.0442
9662.6       0.0482      4991.6     0.0514    2221.9      0.0554      943.22    0.0602
675.30       0.0626      517.66     0.065     378.19      0.0674      221.12    0.0706
154.71       0.073       111.38     0.0762    82.450      0.0802      66.605    0.0874
55.530       0.0946      46.550     0.1045    37.050      0.1245      27.722    0.2075
24.920       0.3075      19.306     0.64      13.253      1.24        9.5504    2.04
7.9420       2.84        4.8772     4.84      2.7097      8.34        1.5627    12.34
1.0540       16.34       .69797     22.34     .56627      26.34       .47391    30.34
.4171        .0254       .5329      .0762     .6364       .1270       .7955     .1778
.8725        .2286       .9575      .2794     1.0038      .3302       1.0347    .3810
1.0501       .4318       1.0193     .4826     .9884       .5334       .9266     .5842
.8493        .6350       .7722      .6858     .6718       .7366       .5560     .7874
.4479        .8382       .3398      .8890
```

```
         1         2         3         4         5         6         7         8
12345678901234567890123456789012345678901234567890123456789012345678901234567890
    2                                  5    3    31
0.0165834
0.00576183
1.2933E-04
1.14         2.12
    1    17              4.650 E-06.1896 E+060.0543   0.008        .00102      300.
0.777        0.223
```

```
                    *** ROD CODE GENERAL INPUT ***
 INPUT IS IN S. I. UNITS
 NUMBER OF FUEL RODS          = 1
 NUMBER OF FLOW CHANNELS      = 1
 NUMBER OF AXIAL NODES        = 12

 FUEL DEFORMATION MODEL TYPE = 3
 FREE THERMAL EXPANSION FUEL DEFORMATION MODEL SPECIFIED

 CATHCART CLADDING OXIDATION MODEL SPECIFIED

 MODIFIED ROSS AND STELTE MODEL FOR GAP CONDUCTANCE TO BE USED

 GAS FLOW MODEL TURNED ON

 BALLOON CALCULATIONS SUPPRESSED(USE FCM1 SUBCODE AFTER CLADDING FAILURE)

 FUEL CONDUCTIVITY CORRECTED FOR CRACKING ACCORDING TO FRAP-S3 FORMULA
 INITIAL TIME          = 0.          SEC
 FINAL TIME            = .10000E+01 SEC

 NORMALIZED AXIAL VARIATION IN FAST FLUX ASSUMED SAME AS THAT OF FUEL ROD POWER

 *** NO GOALS TURNED ON ***

**********************************************************************

********** REFLOOD FLAG IS SET TO OFF **********

**********************************************************************
  SUMMARY OF THE LACE SPECIFICATIONS WITH THE SPECIFIED OPTION     NONE
```

```
                    / THERMAL PROPERTY DATA /

FUEL PROPERTY TABLES IN THE TEMPERATURE RANGE   62.3 TO 5462.3 F          290.0 TO 3290.0 K
WILL USE 100 POINTS FOR THERMAL CONDUCTIVITY, 100 FOR HEAT CAPACITY.

CLAD PROPERTY TABLES IN THE TEMPERATURE RANGE   62 . TO 3662.3 F          290.0 TO 2290.0 K
WILL USE  50 POINTS FOR THERMAL CONDUCTIVITY,  50 . HEAT CAPACITY.

FUEL DENSITY =          6.4975E+02 LBM/FT**3     1.0408E+04 KG/M**3
FRACTION OF THEORETICAL DENSITY = 94.90 %

CLAD DENSITY =          4.0954E+02 LBM/FT**3     6.5602E+03 KG/M**3

GAS GAP HEAT CAPACITY = 1.200E-02 BTU/FT**3.F    8.0488E+02 J/M**3.K

FUEL MELTING TEMPERATURE =  5117.5 F                3098.4 K

FUEL HEAT OF FUSION =   7.6540E+04 BTU/FT**3     2.8518E+09 J/M**3

CLAD MELTING TEMPERATURE =  3317.0 F                2098.2 K

CLAD HEAT OF FUSION =   3.9616E+04 BTU/FT**3     1.4760E+09 J/M**3
ERROR IN PLATE

INITIAL INDEX =    1        FINAL INDEX =    0        ARRAY LENGTH =   13        ARGUMENT =

TABLE OF X VALUES =
  .3000000E+03   .4000000E+03   .6400000E+03   .1090000E+04   .1093000E+04   .1113000E+04   .1133000E
  .1173000E+04   .1213000E+04   .1213000E+04   .1233000E+04   .1240000E+04

LISTING OF INPUT DATA FOR CASE  1

    1    * MESH SENSITIVITY STUDY  10 FUEL MESH SPACINGS
    2    C.C4CCC1   14 2 2.0 1.0 200 0.5 200
    3    C1C1C2CC   0 1
    4    C1C102C1   1 0.CC192   1 0.0027149   1 0.0031835   1 0.0035915   1 0.0037175
    5    C1C102C2   1 2.0038394   1 0.CC39576   1 0.CC4C723   1 0.0041842   1 C.CC4293
    6    C1C102C3   1 0.CC43775   2 0.CC4989
    7    C1C1C3C1   1 10   3 11   2 13
    8    C4C1C4C1   C.9220166 1   0.9853252 2   0.9822CC2 3   1.007017 4   1.023360 5
    9    C1C1C4C2   1.037838 6   1.073251 7   1.110507 8   1.147761 9   1.185014 10
   10    C1C1C4C3   C.C 11   0.CC4 13
   11    C4C106C1   550. 14
   12    *

  GENERAL DATA
      HEAT1 PROBLEM NUMBER    =  1
      NUMBER OF MESH POINTS   =  14
      GEOMETRY TYPE           =  CYLINDRICAL
      LEFT BOUNDARY COORD.    =  0.
      SOURCE SCALING FACTOR   =  1.000000E+00
      TOTAL INTEG. SOURCE     =  6.25236E-04
  DATA FOR STEADY STATE CALCULATIONS
      MAX NO. OF ITERATIONS   =  200
      CONVERGENCE CRITERION   =  9.000000E-01
  DATA FOR TIME DEPENDENT CALCULATIONS
      MAX NO. OF ITERATIONS   =  200
```

*** COOLANT CONDITIONS ***

NSWC = 2 TRANSIENT COOLANT CONDITIONS TO BE OBTAINED FROM AUXILIARY DATA SET 1

3 THERMAL-HYDRAULIC PROGRAM VOLUMES USED TO SPECIFY AXIALLY VARYING COOLANT CONDITIONS ALONG LENGTH

CRITICAL HEAT FLUX OPTION = 3 NO COLD WALL NO AXIAL FACTORS

C - H - F CORRELATION = 3 HUGHES / TONG (W-3)

POST-CHF HEAT TRANSFER CODE = 1 GROENEVELD EQN. 5.7 AS MODE 5.

*** DATA FOR 1 COOLANT CHANNELS ***

CHANNEL NO.	EQUIVALENT HEATED DIAM. (FT)	(M)	EQ. HYDRAULIC DIAMETER (FT)	(M)	FLOW AREA (FT**2)	(M**2)
1	5.4407E-02	1.6583E-02	1.8904E-02	5.7618E-03	1.3921E-03	1.2933E-04

*** GAP CONDUCTANCE SUBCODE INPUT ***

ARITHMETIC MEAN ROUGHNESS OF CLADDING (MICRONS) = .119CE+01

ARITHMETIC MEAN ROUGHNESS OF FUEL (MICRONS) = .212CE+01

*** GAS GAP DATA ***

XXX DATA FOR ROD 1 XXX

MOLES OF GAS IN FUEL ROD COMPUTED FROM INPUT SPECIFIED INITIAL PRESSURE AND TEMPERATURE

INITIAL GAS TEMPERATURE = .803E+02 F .300E+03 K

PLENUM VOLUME = 1.642E-04 FT**3 (4.650E-06 M**3)

GAP PRESSURE = 2.75CE+01 PSIA (1.896E+05 N/M**2)

SPRING LENGTH= 1.781E-01 FT (5.430E-02 M)

COIL OD SPRING = 2.625E-02 FT (8.000E-03 M)

NUMBER OF COILS = 17

WIRE OD OF SPRING = 3.346E-03 FT (1.020E-03 M)

MOLE FRACTIONS OF GAS COMPONENTS

HELIUM	ARGON	KRYPTON	XENON	HYDROGEN	NITROGEN	H2O
.7770E+00	.2230E+00	0.	0.	0.	0.	0.

NUMBER OF GRAM-MOLES OF GAS IN FUEL ROD = 1 = .3455581E-03

COLD STATE VOID VOLUME OF FUEL ROD = .4380 INCH**3 .7178CE+04 MM**3